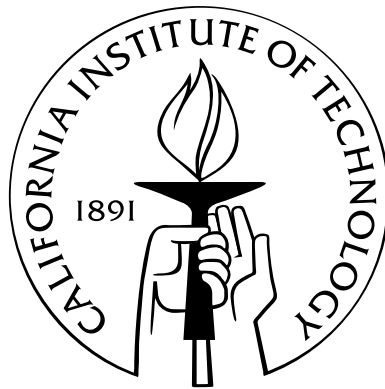


# A Novel Experimental Study of a Valveless Impedance Pump for Applications at Lab-On-Chip, Microfluidic, and Biomedical Device Size Scales

Thesis by  
John Meier

In Partial Fulfillment of the Requirements  
for the Degree of  
Doctor of Philosophy



California Institute of Technology  
Pasadena, California

2011  
(Defended May 23, 2011)



## Acknowledgments

I am very thankful to my advisor, Dr. Mory Gharib, for his mentorship and inspiring creativity and enthusiasm. I would also like to thank the members of my thesis committee: Dr. John Dabiri, Dr. Beverley McKeon, and Dr. Guruswami Ravichandran, for their time, insight, and careful consideration of my work.

It is also important to recognize the contribution of Dr. Derek Rinderknecht, who played an instrumental role in designing many of the experiments carried out in this thesis, and also inspired me to attend Caltech for my graduate studies.

Lastly, I would like to thank my family and friends: in particular my brother, Dr. Steve Meier, for inspiring me to pursue a PhD, my mother Kathy, for always believing in me and expecting the best from me, and my wife Mariko, for being there every day to put things in perspective and support me.

# Abstract

In 1954, Gerhart Liebau demonstrated a simple valveless pumping phenomenon utilizing the periodic compression of a compliant tube and some systematic asymmetry to pump water out of a bucket. Liebau's goal was to explain peculiarities seen in the human circulatory system. In the years that have followed, the Liebau phenomenon has been studied in a variety of open and closed loop configurations, through experimental, computational, and analytical studies.

Recent advances in microfluidic and microelectromechanical systems (MEMS) technology have enabled a wide range of small scale engineering systems. The further development of many important systems is limited by the absence of an appropriate means of fluid transport. Valveless pumps based on the Liebau phenomenon show great promise, particularly in lab-on-chip (LOC), biological, and medical applications in which biocompatibility and the ability to move sensitive molecules without damage are key design requirements.

The purpose of this thesis is to synthesize previous studies of the Liebau phenomenon and produce the first extensive experimental study of a novel valveless pump at size scales and geometries that are relevant to lab-on-chip, microfluidic, and biomedical device applications. For the first time, detailed, dynamic pressure and flow data have been recorded during the operation of these valveless pumps for a large range of operating parameters. This dynamic data allowed us to identify new flow regimes and observe previously undocumented pump behaviors and performance. Parameters investigated include pump material properties and geometry, working fluid density and viscosity, pump excitation properties (amplitude, offset, location, and frequency), and flow loop/system properties. A critical relationship between the relative volumetric compliance of the valveless pump to the system it acts upon is identified, and the implications for practical implementation of valveless pumps at small size scales are discussed.

# Contents

<b>Abstract</b>	<b>iv</b>
List of Figures . . . . .	viii
List of Tables . . . . .	xiii
<b>1 Introduction</b>	<b>1</b>
1.1 Motivation . . . . .	1
1.2 Pumping . . . . .	2
1.3 Microscale Pumping . . . . .	3
1.3.1 Advantages of the Impedance Pump for Microscale Applications . . . . .	5
1.3.1.1 Shear Stress Estimate . . . . .	5
1.3.1.2 Impedance Pump Performance Compared to other Micropumps . . . . .	6
1.4 Liebau Phenomenon Literature Review . . . . .	7
1.4.1 Principal of Operation . . . . .	12
1.4.1.1 Moser’s Impedance-Defined Flow . . . . .	13
1.4.1.2 Mechanical Wave Impedance and Resonance . . . . .	13
1.4.2 Liebau Phenomenon on the Microscale . . . . .	14
1.5 Thesis Objectives . . . . .	15
Bibliography . . . . .	19
<b>2 Experimental Methods and Materials</b>	<b>23</b>
2.1 Experimental Objectives . . . . .	23
2.2 Characterization System . . . . .	23
2.2.1 Loop Resistance . . . . .	24
2.2.2 Equipment Specifications . . . . .	25
2.2.3 Data Acquisition and Filtering . . . . .	25
2.3 Material Properties . . . . .	27
2.3.1 Tube-Based Pumps . . . . .	27
2.3.1.1 Elastic Modulus Measurements . . . . .	27
2.3.2 Planar Sheet Pumps . . . . .	28

2.3.2.1	Elastic Modulus Measurements . . . . .	28
2.3.3	Pumping Element and Loop Compliance . . . . .	29
	Bibliography . . . . .	31
<b>3</b>	<b>Experimental Results</b>	<b>32</b>
3.1	Basic Behaviors . . . . .	32
3.1.1	Wave Speed . . . . .	33
3.1.2	Resonant Frequency . . . . .	35
3.2	Thin-Walled Tube as a Pump . . . . .	37
3.2.1	Excitation Location . . . . .	38
3.2.2	Excitation Amplitude and Offset . . . . .	39
3.2.3	Inlet/Outlet Pressure Condition (Venting) . . . . .	40
3.2.4	Transmural Pressure . . . . .	41
3.2.5	Loop Resistance . . . . .	42
3.2.6	Viscosity Effects . . . . .	43
3.3	Thick-Walled Tube as a Pump . . . . .	44
3.3.1	Excitation Location and Tube Length . . . . .	44
3.3.2	Excitation Amplitude and Offset . . . . .	46
3.3.3	Inlet/Outlet Pressure Condition (Venting) . . . . .	47
3.3.4	Transmural Pressure . . . . .	48
3.3.5	Loop Resistance . . . . .	49
3.3.6	Viscosity Effects . . . . .	50
3.4	Planar Pumps . . . . .	51
3.4.1	Excitation Location . . . . .	51
3.4.2	Inlet/Outlet Pressure Condition (Venting) . . . . .	52
3.4.3	Elastic Modulus Effects . . . . .	53
3.4.4	Viscosity Effects . . . . .	54
	Bibliography . . . . .	55
<b>4</b>	<b>Discussion and Analysis</b>	<b>56</b>
4.1	Reynolds Number and Womersley Number Scaling . . . . .	56
4.2	Transient Behaviors at Startup and Relaxation . . . . .	57
4.2.1	Startup . . . . .	57
4.2.2	Relaxation . . . . .	59
4.3	Comparison to Previous Studies . . . . .	60
4.4	Pump Curve . . . . .	63
4.5	Viscosity and Density . . . . .	63

4.6	Efficiency . . . . .	64
4.6.1	Volumetric Efficiency . . . . .	64
4.6.2	Pump Power and Efficiency . . . . .	65
4.6.2.1	Inefficiency Leading to Heating of the Working Fluid . . . . .	66
4.7	Offset and Amplitude . . . . .	66
4.8	Transmural Pressure . . . . .	67
	Bibliography . . . . .	68
<b>5</b>	<b>Conclusion</b>	<b>69</b>
5.1	Summary of Important Findings . . . . .	69
5.2	Future Directions . . . . .	72
5.2.1	Computational Modeling . . . . .	72
5.2.2	Membrane Tracking using DDPIV . . . . .	72
5.2.3	Attached Actuators . . . . .	72
5.2.4	Other Valveless Pumping Scenarios of Interest . . . . .	73
5.2.4.1	Ocean Wave Energy Capture . . . . .	73
5.2.4.2	Impedance Pump with Valves . . . . .	73
	Bibliography . . . . .	74
<b>A</b>	<b>Data Acquisition System Verification</b>	<b>75</b>
<b>B</b>	<b>Viscosity Sample Verification</b>	<b>77</b>
<b>C</b>	<b>DDPIV</b>	<b>79</b>
	Bibliography . . . . .	81
<b>D</b>	<b>Wave Rectifying Water Channel: Liebau Phenomenon on a Free Surface</b>	<b>82</b>
D.1	Experiment . . . . .	82
D.2	Wave Generation and Data Collection . . . . .	83
D.3	Frequency Sweep Results . . . . .	84
	Bibliography . . . . .	87
<b>E</b>	<b>Pump Behavior with Valves</b>	<b>88</b>
E.1	Valve Characterization . . . . .	88
E.2	Effect of Single and Multiple Valves on Performance . . . . .	88

# List of Figures

1.1	Two methods of flow rectification employed in fixed-geometry valveless pumps. Figure adapted from Nabavi (2009) . . . . .	4
1.2	Forouhar et al. (2006) showed that at frequencies of 1.7 Hz and 2.3 Hz, the flow performance of the zebra fish valveless heart tube increased, likely due to resonant wave interactions and flow development based on the Liebau phenomenon. Figure adapted from Forouhar et al. (2006) . . . . .	5
1.3	Comparison of various micropumps based on maximum flow rate $Q_{max}$ , maximum pressure $\Delta p_{max}$ , and package size $S_p$ . The micropump references noted in the figure can be found in Laser and Santiago (2004). Figure adapted from Laser and Santiago (2004) . . . . .	7
1.4	Liebau's first physical model of the valveless pumping concept. Region 1 is a 40 cm long elastic tube with a 1 cm inner diameter, Region 2 is a 160 cm long elastic tube with a 0.25 cm inner diameter, Region 3 is a conical glass coupler for the two tubes, and Region 4 is bucket from which water was extracted using a rhythmic compression of the larger diameter tube at Region 5. Figure adapted from Liebau (1954b) . . . . .	8
1.5	Takagi's rigid T-junction valveless pumping experiment and the open loop compliant experiment (essentially the modern impedance pump) originally studied by Bredow and Rath. Figure adapted from Takagi and Saijo (1983) and Rath and Teipel (1978) . . . . .	9
1.6	Moser's distensible reservoir physical model and equivalent lumped parameter electrical circuit model. Figure adapted from Moser et al. (1998) . . . . .	10
1.7	Borzi's numerical study is able to predict the behavior around resonance seen in the experimental study of a rigid asymmetric T-junction system studied by Takagi. In both plots, the y-axis is the average pressure head developed across the pump and the x-axis is the excitation frequency normalized by the natural frequency of the system. Here natural frequency is defined as the frequency of free oscillation from a small perturbation to the pressure. Figure adapted from Takagi and Takahashi (1985) and Borzi and Propst (2003) . . . . .	11

1.8	Avrahami and Gharib (2008) performed a control volume analysis to show that the passive section of the pump was actually doing useful work on the fluid at resonance conditions. Figure adapted from Avrahami and Gharib (2008) . . . . .	12
1.9	A schematic of an impedance pump, where the compliant tube has an impedance $Z_o$ and is coupled at either end to rigid tubes with impedance $Z_1$ and $Z_2$ . Typically, $Z_1 = Z_2$ , but the important condition for wave reflection in the pump is that $Z_1$ and $Z_2$ are different than $Z_o$ . . . . .	14
1.10	Top left shows the experimental setup of Hickerson (2005) and going clockwise are five micropump prototypes from Rinderknecht (2008) including a 2 mm electromagnetically actuated pump, 1 mm electromechanically actuated pump, a 200 $\mu\text{m}$ electromagnetically actuated planar pump, a 250 $\mu\text{m}$ piezoelectrically actuated planar pump, and a 350 $\mu\text{m}$ electromagnetically actuated pump. Images courtesy of Anna Hickerson and Derek Rinderknecht. . . . .	15
2.1	Experimental characterization system . . . . .	24
2.2	The effect of a 3rd-order Butterworth filter with a 160 Hz (1005.3 rad/s) cutoff frequency on the gain and phase of frequency content in sampled data . . . . .	26
2.3	Tube-based pumps prepared for the characterization system . . . . .	27
2.4	Planar pump frame with dimensioned schematic . . . . .	28
2.5	Elastic modulus measurements of planar elastic membranes. HT6135/White ( $E = 1.4$ MPa), HT6220/Black ( $E = 0.73$ MPa), HT6210/Grey ( $E = 0.36$ MPa) . . . . .	29
3.1	Schematic of a general test in the characterization system show system variable definitions. The valves shown act to open the loop to atmospheric pressure or allow a water column to be placed on the loop to increase the transmural pressure. Flow freely moves around the loop whether these valves are open or closed. . . . .	32
3.2	Example of phase lag between the two pressure transducers due to a finite and measurable wave speed in the fluid filled elastic tube . . . . .	34
3.3	Example data set from the excitation of the Latex Thin tube. ( $x = 5$ mm, $y = 1$ mm, $A = 0.4$ mm, valves = right valve open with .45 kPa water column) . . . . .	37
3.4	Latex Thin tube performance as a function of excitation location. ( $y = 1$ mm, $A = 0.4$ mm, valves = right valve open with .45 kPa water column) . . . . .	38
3.5	Latex Thin tube performance as a function of excitation amplitude and offset. ( $x = 5$ mm, $y = 1$ mm and variable, $A = 0.4$ mm and variable, valves = right valve open with .45 kPa water column) . . . . .	39
3.6	Latex Thin tube performance as a function of inlet pressure conditions. ( $x = 5$ mm, $y = 1$ mm, $A = 0.4$ mm) . . . . .	40

3.7	Latex Thin tube performance as a function transmural pressure. ( $x = 5$ mm, $y = 1$ mm, $A = 0.4$ mm, valves = left valve open with various water columns) . . . . .	41
3.8	Latex Thin tube performance as a function of loop resistance. ( $x = 5$ mm, $y = 1$ mm, $A = 0.4$ mm, valves = right valve open with .45 kPa water column) . . . . .	42
3.9	Latex Thin tube performance as a function of fluid viscosity. ( $x = 5$ mm, $y = 1$ mm, $A = 0.5$ mm, valves = right valve open with .45 kPa fluid column) . . . . .	43
3.10	ABThick-2cm, ABThick-3cm, and ABThick-4cm tubing excited at various positions. ( $x =$ variable, $y = 1$ mm, $A = 0.4$ mm, valves = closed) . . . . .	44
3.11	DOW006-2cm tubing excited at various positions. ( $x =$ variable, $y = 1.1$ mm, $A = 0.4$ mm, valves = both open) . . . . .	45
3.12	ABThick-2cm tube performance as a function of excitation amplitude and offset. ( $x = 5$ mm, $y = 1$ mm and variable, $A = 0.4$ mm and variable, valves = closed) . . . . .	46
3.13	DOW006-2cm tube performance as a function of variable inlet and outlet pressure conditions ( $x = 5$ mm, $y = 1.1$ mm, $A = 0.4$ mm, valves = variable) . . . . .	47
3.14	ABThick-3cm tube performance as a function of variable inlet and outlet pressure conditions and excitation position ( $x =$ variable, $y = 1$ mm, $A = 0.4$ mm, valves = variable) . . . . .	47
3.15	ABThick-2cm tube performance as a function of transmural pressure ( $x = 5$ mm, $y = 1$ mm, $A = 0.4$ mm, valves = left open with variable water column) . . . . .	48
3.16	ABThick-2cm tube performance as a function of loop resistance. ( $x = 5$ mm, $y = 1$ mm, $A = 0.4$ mm, valves = closed) . . . . .	49
3.17	ABThick-2cm tube performance as a function of fluid viscosity. ( $x = 5$ mm, $y = 1$ mm, $A = 0.4$ mm, valves = closed) . . . . .	50
3.18	Planar White-Stiff membrane (1.4 MPa) performance as a function of excitation location ( $x =$ variable, $y = .5$ mm, $A = 0.4$ mm, valves = closed) . . . . .	51
3.19	Planar White-Stiff membrane (1.4 MPa) performance as a function of variable inlet and outlet pressure conditions ( $x = 5$ mm, $y = .5$ mm, $A = 0.4$ mm, valves = variable) . . . . .	52
3.20	Planar pump performance as a function of variable membrane elastic modulus ( $x = 5$ mm, $y = .5$ mm, $A = 0.4$ mm, valves = closed) . . . . .	53
3.21	Planar White-Stiff membrane (1.4 MPa) performance as a function of fluid viscosity( $x = 5$ mm, $y = .5$ mm, $A = 0.4$ mm, valves = closed) . . . . .	54
4.1	The startup of the Latex Thin tube excited at 65 Hz ( $x = 5$ mm, $y = 1.2$ mm, $A = 0.4$ mm, vents = closed) . . . . .	58
4.2	The startup of the DOW006-2cm tube excited at 25 Hz ( $x = 5$ mm, $y = 1.1$ mm, $A = 0.4$ mm, vents = right open) . . . . .	59

4.3	The relaxation of the Latex Thin tube after being excited at 65 Hz ( $x = 5$ mm, $y = 1.2$ mm, $A = 0.4$ mm, vents = closed) . . . . .	59
4.4	The relaxation of the DOW006-2cm tube after being excited at 25 Hz ( $x = 5$ mm, $y = 1.1$ mm, $A = 0.4$ mm, vents = right open) . . . . .	60
4.5	Note that the definition of differential pressure for this study has been inverted to match that of Takagi . . . . .	61
4.6	Pump curve for thin-walled elastic tube under five different operating conditions (distinct loop resistances) . . . . .	63
4.7	All three pump tests shown above were performed with the following parameters: $x = 5$ mm, $y = 1.1$ mm, and $A = 0.4$ mm (0.8 mm total displacement). The right vent was open for the two thick-walled cases, and the loop was closed for the thin-walled case. . . . .	64
4.8	The effect of excitation amplitude and offset on net flow rate for a thin-walled tube excited at 60 Hz and a thick-walled tube excited at 30 Hz. During offset variation, the amplitude was held fixed at 0.4 mm and during amplitude variation, the offset was held fixed at 1.0 mm. . . . .	67
A.1	Verification of DAQ Settings. The imposed high voltage signal does not bleed into the other data acquisition channels. . . . .	76
B.1	Normalized viscosity and density showing the temperature dependence of water and glycerine solutions . . . . .	78
B.2	Verification of measured sample viscosities compared to published data . . . . .	78
C.1	Geometric diagram used for ray tracing and deriving the single lens out-of-plane DDPIV sensitivity equations in Willert and Gharib (1992) . . . . .	79
C.2	Results of the out-of-plane sensitivity calibration for various objective lenses and aperture masks . . . . .	80
C.3	Geometric diagram used for ray tracing and deriving the double lens (microscope) out-of-plane DDPIV sensitivity equations . . . . .	81
D.1	Water tunnel dimensions. $h(t)$ has a minimum value of 1 cm and a maximum value of 1.8 cm . . . . .	83
D.2	A variety of flow regimes exist in the WRWC when only the input frequency is varied . . . . .	84
D.3	Frequency response of the WRWC showing both the mean flow and the amplitude of the oscillatory component . . . . .	85
D.4	The flow rate in the WRWC normalized by the rate of fluid displacement of the plunger . . . . .	85
D.5	Changing the amplitude of the plunger motion has similar effects to tube based impedance pumps . . . . .	86

E.1	Characterization of the Qosina-80057 Duckbill Check Valve. . . . .	88
E.2	Thick-walled AB 2 cm long tube excited at various locations with dummy tubing in place where valves can be added . . . . .	89
E.3	Thick-walled AB 2 cm long tube excited at various locations with various valve configurations . . . . .	90

# List of Tables

1.1	Impedance pump parameter space . . . . .	16
2.1	Loop resistance measurements . . . . .	25
2.2	Sensor specifications . . . . .	25
2.3	Linear actuator specifications . . . . .	25
2.4	Pumping element and flow loop properties . . . . .	30
3.1	Results presented in this chapter . . . . .	33
3.2	Summary of wave speed and resonant frequency measurements. Values with a range represent the uncertainty in the measurement due to the limited resolution of the DAQ timing. . . . .	36
4.1	Summary of characteristic Reynolds numbers for the pumping elements and the flow loop with water as a working fluid . . . . .	57
B.1	Results of viscosity measurements . . . . .	77

# Chapter 1

## Introduction

### 1.1 Motivation

Advances in microfluidics and microelectromechanical systems (MEMS) technology over the past two decades have enabled a wide range of small scale engineering systems. However, the further development of many important technologies is limited by the absence of an appropriate means of fluid transport. Valveless pumps based on the Liebau phenomenon show great promise, particularly in lab-on-chip (LOC), biological, and medical applications in which biocompatibility and the ability to move sensitive molecules without damage are key design requirements.

The Liebau phenomenon is a form of valveless pumping that utilizes the periodic compression or excitation of a compliant tube and some systematic asymmetry to generate significant flow rates (Liebau, 1954a,b, 1955a,b, 1956, 1963). Moser et al. (1998) suggested that the Liebau phenomenon develops a net flow rate through a mechanism called *impedance-defined flow*: that a fluid will take the path of least instantaneous resistance across a dynamic pressure gradient, or the path of lowest *impedance*. Further study of the Liebau phenomenon in a variety of geometries, eventually led to the specific definition of *impedance pump* as a stand-alone actuation scheme and compliant pumping region coupled to a rigid flow loop or fluid reservoirs. Hickerson et al. (2005) were the first to use the term impedance pump, and referred to a different, though equally important definition of impedance. Hickerson et al. (2005) recognized that the wave dynamics in the compliant pumping region and the wave reflections at its ends, where a mechanical wave impedance mismatch occurs, played a critical role in determining the resonance conditions where high flow rates are observed.

Such pumps have no internal machinery, can be constructed from a variety of materials and geometries, and are not required to ever fully occlude the flow, making them well suited to applications with biocompatibility requirements. However, the successful design of an engineering system using this valveless pumping technique requires a comprehensive understanding of the pump dynamics

and expected performance, and there has been very little study to date of the Liebau phenomenon at the size scale in question.

The purpose of this thesis is to synthesize previous studies of the Liebau phenomenon and provide an experimental study of a novel valveless pump, based on the impedance pump concept, at size scales and geometries that are relevant to lab-on-chip, microfluidic, and biomedical device applications. For the first time, detailed, dynamic pressure and flow data has been recorded during the operation of an impedance pump for a large range of operating parameters. This dynamic data allowed us to identify new flow regimes and observe previously undocumented pump behaviors and performance. The data also provides critical transient pressure and flow information that will help validate future computational modeling efforts.

## 1.2 Pumping

Pumps are a fundamental component of many engineering systems as well as a critical life-sustaining component of almost every organism on the planet. In fact, Forouhar et al. (2006) and Maenner et al. (2010) investigated how the valveless embryonic heart tube is able to pump blood based on the Liebau phenomenon at the very earliest stages of life.

At its most basic level, a pump is a device or mechanism that performs useful work by moving a fluid. To move the fluid in a real system, a pressure increase must be achieved to generate the necessary pressure gradient to drive a flow. The power output of a pump is the product of the pressure increase across the pump and the flow rate through the pump. Every pump will have a maximum pressure gradient (at zero flow rate) and maximum flow rate (at zero pressure gradient, though this condition is not physically possible). Real operating conditions of the pump will always lie somewhere between these two extreme values, otherwise no useful work is achieved.

There are as many ways to pump fluid as our imagination permits, so it is useful to try to categorize pumps. Pumps are often categorized by the manner through which they add energy to the fluid, and then further subcategorized by the means in which this principle is implemented (Karassik, 1986). At the highest level, all pumps are categorized as either displacement pumps or dynamic pumps.

- 1 Dynamic pumps: Energy is *continuously* added to increase the fluid velocities within the pump to values greater than those at discharge, so that subsequent velocity reduction within or beyond the pump leads to a pressure increase. Dynamic pumps can be further subcategorized

as follows.

- i Centrifugal
  - ii Special effect
    - Jet pumps
    - Gas lift pumps
    - Etc.
- 2 Displacement pumps: Energy is added *periodically* by the application of force to one or more movable boundaries, resulting in a *direct* increase of pressure to the magnitude required to move the fluid through *valves* or *ports* into the discharge line. Displacement pumps can be further subcategorized as follows.
- i Reciprocating
  - ii Rotary

The reader is likely most familiar with larger scale pumps encountered in everyday life, such as the human heart (reciprocating displacement pump), a supercharger on an automobile engine (centrifugal dynamic pump), or a manually operated bicycle tire pump (piston displacement pump). For the purposes of this thesis, I will focus on the pumping needs of small scale systems such as biomedical devices, lab-on-chip (LOC) technologies, and other microfluidic devices.

### 1.3 Microscale Pumping

Recent advances in microfluidics and microelectromechanical systems (MEMS) technology have enabled a wide range of small scale engineering systems with unique pumping needs. Laser and Santiago (2004) provide an excellent review of both pumping needs and pumping solutions implemented on the microscale. Laser and Santiago (2004) categorize micropumps using the same methods as Karassik (1986), as either displacement pumps or dynamic pumps. However, the fluid physics at the microscale opens up many new possibilities for subcategories. Special effect dynamic pumps at the microscale include electrohydrodynamic, electro-osmotic, magnetohydrodynamic, and acousting streaming pumps. The microscale is an ideal setting for exploiting fluid physics like surface tension and thermocapillary forces in aperiodic displacement pumps (Laser and Santiago, 2004).

One particularly interesting microscale pump that does not have a macroscale counterpart is the fixed-geometry valveless pump. Laser and Santiago (2004) categorize this pump as a fixed-geometry, reciprocating diaphragm, displacement pump. Many fixed-geometry valveless pumps have been fabricated on the microscale and the concept was extensively reviewed by Nabavi (2009). Figure 1.1

shows two different schemes for achieving a net flow in these pumps based on directional bias in flow resistance attained through rigid geometric features.

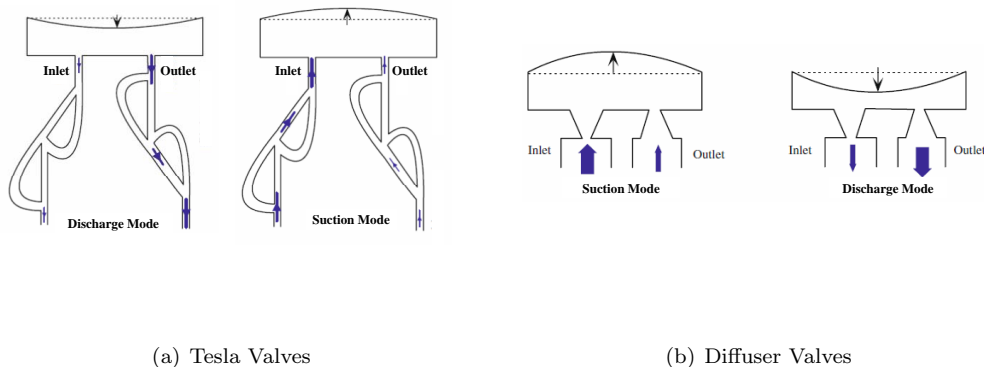


Figure 1.1: Two methods of flow rectification employed in fixed-geometry valveless pumps. Figure adapted from Nabavi (2009)

Fixed-geometry valveless pumps are actually a special, constrained case of the more general valveless pumping effect known as the Liebau phenomenon. Fixed-geometry valveless pumps rectify flow using the difference in resistance depending on flow direction across a nozzle-diffuser element or a Tesla valve. However, its use of rigid geometric features prevents many rich dynamical behaviors that have been seen in less constrained, compliant tube devices based on the Liebau phenomenon. For instance, the impedance pump, which uses a compliant tube, changes in mechanical wave impedance, wave propagation and reflection, and resonance to rectify the flow, has been shown to reverse flow direction by simply changing the excitation frequency. Flow reversal based on frequency does not occur in nozzle-diffuser elements or Tesla valves, because their rigid, fixed-geometry defines the preferred path for flow. Flow through a fixed-geometry pump increases linearly with frequency up to the point where the losses in either direction become comparable and the flow rectification performance declines (Olsson et al., 1997). The rich dynamics, like frequency dependent flow reversal, of the more general Liebau phenomenon could be extremely useful to engineers trying to design practical microscale devices.

The more general Liebau phenomenon was not reviewed by Laser and Santiago (2004) due to the lack of work done at the microscale at the time of publication. However, Forouhar et al. (2006) provided the inspiration for exploring the use of a compliant tube micropump based on the Liebau phenomenon when they showed that the embryonic zebra fish circulated blood using a localized contraction, wave propagation, and wave reflection in a valveless heart tube with an inner diameter

on the order of  $50\ \mu\text{m}$ . Figure 1.2 clearly distinguishes the flow behavior in the valveless heart tube from the previously assumed peristaltic mechanism, by showing performance above that expected for a peristaltic mechanism for frequencies of 1.7 Hz and 2.3 Hz.

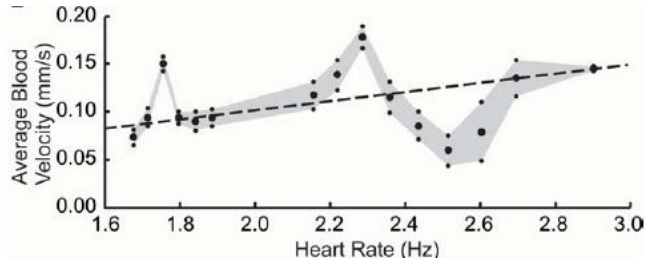


Figure 1.2: Forouhar et al. (2006) showed that at frequencies of 1.7 Hz and 2.3 Hz, the flow performance of the zebra fish valveless heart tube increased, likely due to resonant wave interactions and flow development based on the Liebau phenomenon. Figure adapted from Forouhar et al. (2006)

Inspired by the results of Forouhar et al. (2006), Rinderknecht et al. (2005) fabricated the first microscale pump based on the Liebau phenomenon using a polyurethane tube with a  $250\ \mu\text{m}$  inner diameter and  $50\ \mu\text{m}$  wall thickness. Using an 82 Hz excitation, Rinderknecht et al. (2005) was able to generate a flow rate of approximately  $17\ \mu\text{l}/\text{min}$  ( $Re \approx 2$ ) while pumping between two water droplets. Later, Rinderknecht (2008) studied the frequency vs. flow behavior of a 1.9 mm inner diameter latex pump and observed many flow behaviors previously observed on large scale versions of the Liebau phenomenon, including apparent resonant behavior and frequency dependent flow reversals.

### 1.3.1 Advantages of the Impedance Pump for Microscale Applications

Rinderknecht (2008) suggested that the valveless impedance pump was particularly well suited for microscale applications, due to its simple geometry and ease of fabrication compared to other micropumps. The fabrication techniques used for microscale impedance pumps would be essentially identical to those for reciprocating diaphragm displacement pumps, however the most complicated step in current displacement pump fabrication, valve fabrication, is not necessary in impedance pumps. The impedance pump also has the benefit of no internal moving parts, blades, valves, or high electric fields making the pump safer for studies involving sensitive molecules.

#### 1.3.1.1 Shear Stress Estimate

Rinderknecht et al. (2005) suggested that the relatively low shear stresses in the impedance pump make it well suited for pumping sensitive molecules. It is useful to estimate the shear stress in the pump to verify this claim. Equation 1.1 represents the shear stress,  $\tau$ , for a Newtonian fluid with

dynamic viscosity  $\mu$  and velocity gradient  $\frac{\partial u}{\partial y}$ .

$$\tau = \mu \frac{\partial u}{\partial y} \quad (1.1)$$

The highest flow rates seen in the studies presented in this thesis were on the order of 10 mL/min, corresponding to velocities of 9.4 cm/s for tubing with 1.5 mm inner diameter. Therefore, the highest shear rates were likely seen at the point of actuation where maximum wall velocities were 25 cm/s for a typical 0.4 mm amplitude excitation at 100 Hz. Using this maximum velocity and assuming a velocity gradient length scale of 0.75 mm (smallest inner radius of tubing) and fluid viscosity of  $1e10^{-3}$  Pa\*s (water at 20 °C), the estimated shear stress is 0.33 Pa, well below the value of 150 Pa where human red blood cells start to experience damage due to shear stress (Leverett et al., 1972).

This shear stress estimate for a given pump will increase linearly with increases in fluid viscosity, frequency, and amplitude of excitation. It will also increase linearly with decreases in characteristic length (i.e. decreasing radius/size scales). If the pump phenomenon is scaled down, (excitation amplitude)/(pump characteristic radius) and (excitation frequency)/(pump characteristic radius) will be relatively constant, so the shear stress would be expected to increase linearly with decreasing size scales. This scaling indicates that clogging due to internal pump diameters on the order of blood cell diameters ( 10  $\mu$ m) will occur on the same size scales as damage caused by shear stress in the fluid, verifying that the impedance pump is a good candidate micropump for use with sensitive particles.

### 1.3.1.2 Impedance Pump Performance Compared to other Micropumps

The metric used by Laser and Santiago (2004) to compare micropump performance across size scales and mechanisms was the self-pumping frequency,  $f_{sp}$ , defined by Equation 1.2.  $S_p$  is the overall volume of the pump and  $Q_{max}$  is the maximum flow rate of the pump.

$$f_{sp} = \frac{Q_{max}}{S_p} \quad (1.2)$$

In the review by Laser (2004), the self-pumping frequency of 20 different micropumps with various operating principles were plotted versus the micropump package size. The impedance pumps studied in this thesis fall in the middle of the range for package size and near the top end of self-pumping frequency. The self-pumping frequency of the planar impedance pump studied in this thesis is very similar to the valveless diffuser pump studied by Olsson et al. (1997). The maximum pressure differential,  $\Delta p_{max}$ , of the impedance pump is on the lower end of standard micropumps due to its lack of valves, which are useful for fighting back pressures, but still within the same range as many other micropumps.

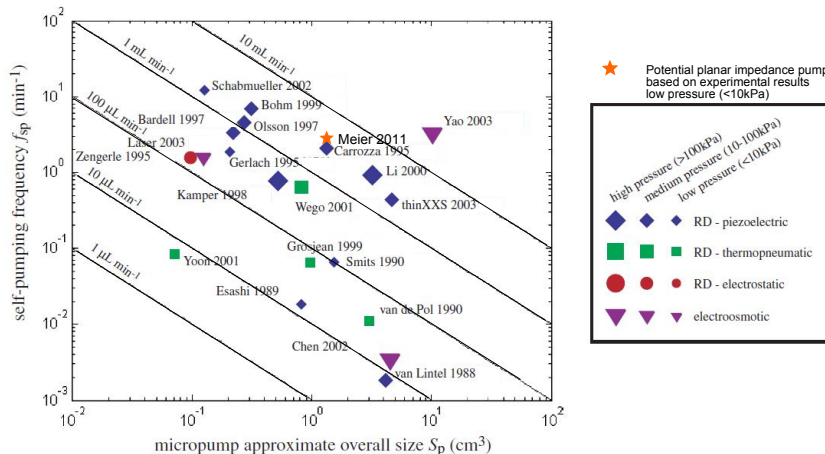


Figure 1.3: Comparison of various micropumps based on maximum flow rate  $Q_{max}$ , maximum pressure  $\Delta p_{max}$ , and package size  $S_p$ . The micropump references noted in the figure can be found in Laser and Santiago (2004). Figure adapted from Laser and Santiago (2004)

## 1.4 Liebau Phenomenon Literature Review

The impedance pump, the Liebau phenomenon, and valveless pumping in general have been investigated by a variety of experimental, analytical, and modeling studies since Liebau's first work in 1954. Liebau's motivation for investigating valveless pumping stemmed from his skepticism, like that of many other scientists, that the human heart could maintain blood circulation throughout the entire body on its own. Liebau was the first scientist to propose a physical model for how muscle contractions, or crosstalk between pulsating arteries and veins, could lead to a valveless pumping mechanism. Figure 1.4 shows Liebau's schematic of the first physical model for valveless pumping, with which he was able to pump water out of a bucket through rhythmic compression of a large diameter elastic tube coupled to a smaller diameter elastic tube.

In future studies, Liebau simplified his valveless pumping concept to a flow loop consisting of a large diameter elastic tube, excited asymmetrically, coupled to a small diameter glass tube, creating a circular flow loop that would be studied again and again by future researchers (Liebau, 1955b). While the results of Liebau's experiments were mostly qualitative observations, he did identify the mechanical and geometric properties of the tubes, the fluid properties, and the asymmetric compression point as critical factors in driving the flow. Interestingly, Liebau (1955b) also considered the directional dependence on flow resistance through nozzle/diffuser elements and noted their existence in the circulatory systems of many living things.

A modest collection of experimental works on the Liebau phenomenon has followed this initial

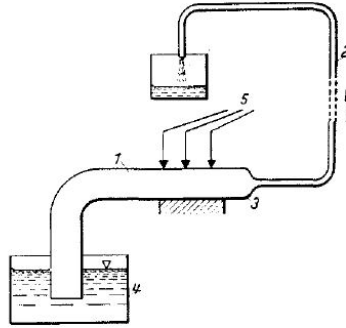


Figure 1.4: Liebau's first physical model of the valveless pumping concept. Region 1 is a 40 cm long elastic tube with a 1 cm inner diameter, Region 2 is a 160 cm long elastic tube with a 0.25 cm inner diameter, Region 3 is a conical glass coupler for the two tubes, and Region 4 is bucket from which water was extracted using a rhythmic compression of the larger diameter tube at Region 5. Figure adapted from Liebau (1954b)

work. Mahrenhotlz (1963) recreated Liebau's circular flow loop to compare to a simple lumped-parameter mathematical model. Bredow (1968) created an open loop version of Liebau's system, connecting two reservoirs with a compliant tube and rhythmically exciting the system with a flat plate. Bredow confirmed the previous observations about a need for asymmetry, but also noted a performance dependence on the excitation amplitude and frequency. Rath and Teipel (1978) continued the experimental study of Bredow's open loop system, looking at the head developed between two reservoirs for a range of excitation frequencies. Rath was the first to note that a reversal in the sign of the pressure head can actually be achieved simply by changing the frequency of actuation. Takagi and Saijo (1983) developed a simple T-junction system of pipes that was able to replicate valveless pumping in a rigid system by creating the asymmetric resistance using different lengths of pipes on either side of the T-junction. Inspired by the frequency dependence seen in Bredow's work, Takagi and Takahashi (1985) then investigated the rigid T-junction system near resonance conditions and were able to experimentally recreate the frequency dependent flow direction seen by Rath. Figure 1.5 shows a schematic of Takagi's experiment compared to the open loop systems studied by Bredow and Rath.

More recently, several studies have carried out simple experimental observations on systems designed to complement more complex computational or modeling efforts (Ottesen, 2003; Bringley et al., 2008; Wang, 2011). The most extensive experimental study, before the work presented in this thesis, is that of Hickerson (2005) and Hickerson et al. (2005). Hickerson performed a parametric study of a 15 cm long, 1.9 cm inner-diameter polyethylene tube in what was essentially the open loop configuration seen in Bredow (1968). In part of the study, flow was allowed between the reservoirs at either end of the pump, creating a closed loop scenario that did not transfer fluid momentum



was the first to go beyond a simple lumped-parameter model. Thomann used the method of characteristics to study a system very similar to the torus-shaped loop investigated experimentally by Liebau and Mahrenholz. Thomann assumed the model could be cut open in the rigid section and treated as a periodic entity, and his results predicted a net flow for a system with an inviscid and incompressible fluid. However, the simplifying assumptions prevented Thomann's model from explaining other valveless pumping behaviors, like reversal of the direction of net flow with changing excitation frequency.

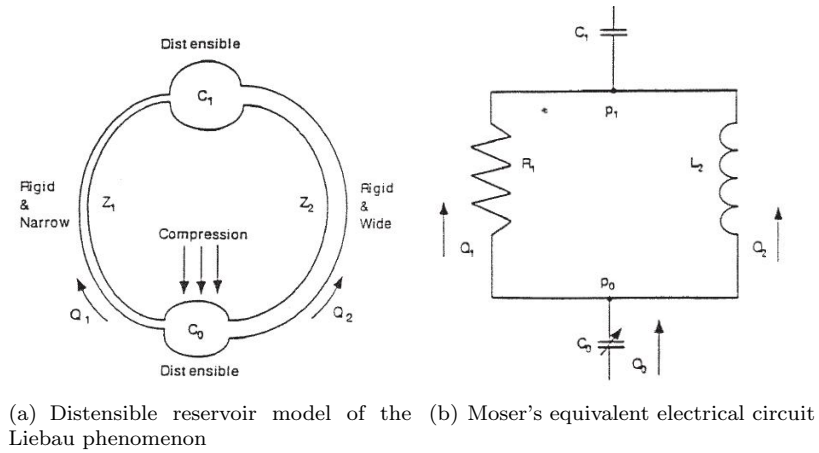


Figure 1.6: Moser's distensible reservoir physical model and equivalent lumped parameter electrical circuit model. Figure adapted from Moser et al. (1998)

Many other mathematical models have followed, each of which including simplifying assumptions to study specific behaviors seen in valveless pumping (Jung and Peskin, 2001; Auerbach et al., 2004; Manopoulos et al., 2006; Propst, 2006; Jung et al., 2008; Avrahami and Gharib, 2008; Loumes et al., 2008; Lee and Jung, 2008; Timmermann and Ottesen, 2009; Lee et al., 2009; Babbs, 2010; Lim and Jung, 2010; Rosenfeld and Avrahami, 2010; Lim and Jung, 2010; Shin and Sung, 2010). It is an interesting problem to model because it contains fluid-structure interactions, wave propagation, and counterintuitive behaviors. Each of these studies provides new results and insights into valveless pumping, but none has shed light on the potential scaling effects of implementing the device on size scales relevant to microfluidic applications.

In two examples of investigations into specific behaviors, Kenner et al. (2000) looked at the role of asymmetry and Hickerson and Gharib (2006) developed a simple wave pulse model to predict resonant frequency behaviors. One of the more extensive numerical investigations was carried out by Borzi and Propst (2003) and investigates both the open loop rigid T-junction case first proposed by Takagi and Saijo (1983) and the open loop compliant case studied by Rath and Teipel (1978)

and Bredow (1968). Borzi was able to predict the flow behavior observed by Takagi and Takahashi (1985) around the resonant frequency of the system, with a switch from high negative head to high positive head as the excitation frequency passes through the resonant frequency, here defined as the frequency of free oscillation from a small perturbation. Figure 1.7 shows the comparison between Takagi's experimental and Borzi's numerical results.

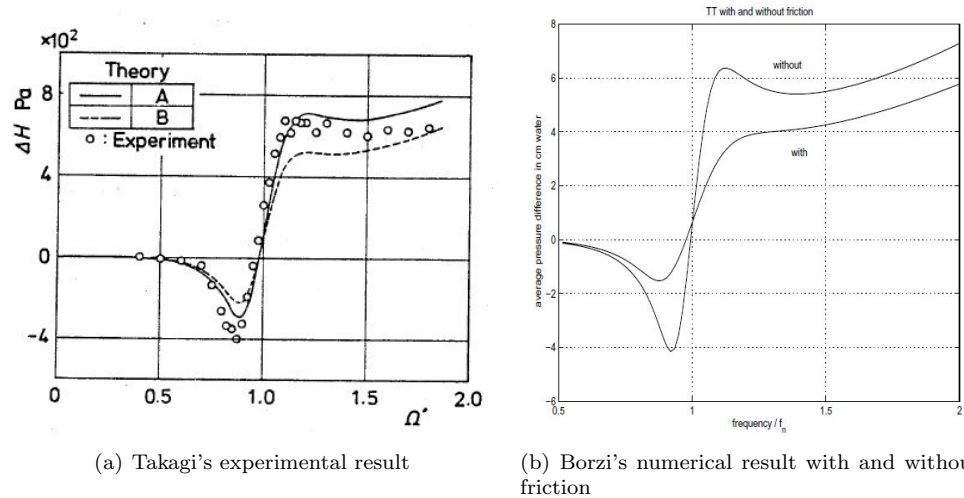


Figure 1.7: Borzi's numerical study is able to predict the behavior around resonance seen in the experimental study of a rigid asymmetric T-junction system studied by Takagi. In both plots, the y-axis is the average pressure head developed across the pump and the x-axis is the excitation frequency normalized by the natural frequency of the system. Here natural frequency is defined as the frequency of free oscillation from a small perturbation to the pressure. Figure adapted from Takagi and Takahashi (1985) and Borzi and Propst (2003)

In one of the more recent and comprehensive, computational studies, Avrahami and Gharib (2008) use an axisymmetric, numerical model with parameters similar to the experimental study of Hickerson (2005). Avrahami and Gharib (2008) were able to recreate the resonant flow peaks seen in Hickerson (2005), but other behaviors, notably flow reversal with changing excitation frequency, are not observed. Avrahami's comprehensive study included a detailed analysis of pressure and flow conditions along the length of the pump, and an energy analysis for a control volume in the longer section of the pump. Using this control volume analysis, shown in Figure 1.8, Avrahami and Gharib (2008) observed that at the highest net flow rate conditions, the passive section of the pump was actually performing useful work on the fluid and increasing the sum of the output kinetic and potential energy. Avrahami and Gharib (2008) identify a *pumping region* towards the end of the long passive section of the pump that includes the location of mechanical wave impedance mismatch, where incoming and reflected waves interact. The hypothesis set forth by Avrahami and Gharib (2008) is that at resonant conditions, these interacting waves create sudden expansions of the

pump near the impedance mismatch and a corresponding pressure driven flow wave out of the pump.

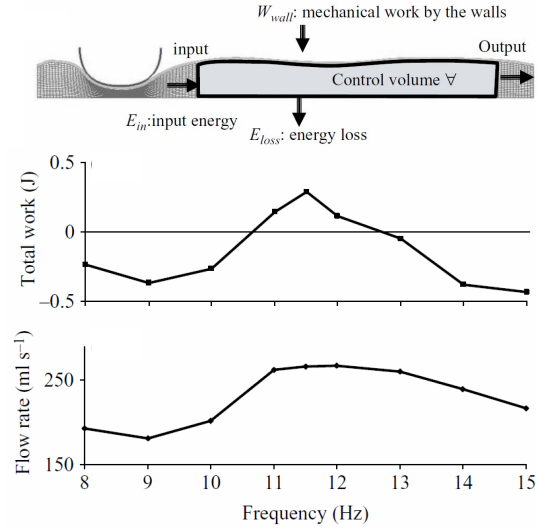


Figure 1.8: Avrahami and Gharib (2008) performed a control volume analysis to show that the passive section of the pump was actually doing useful work on the fluid at resonance conditions. Figure adapted from Avrahami and Gharib (2008)

Avrahami and Gharib (2008) used Equation 1.3 to represent the total work done by the pump wall on the fluid for one period of a steady-state, periodic operating condition.  $W_{pump}$  is the total energy added to the fluid in the control volume in the long passive region of the pump.  $\dot{W}_{wall}$  is the rate of work done by the wall on the fluid,  $\dot{E}_{loss}$  is the rate energy is lost to viscous dissipation,  $\dot{E}_{in}$  represents the rate of kinetic and potential energy entering the control volume on the left side, and  $\dot{E}_{out}$  represents the rate of kinetic and potential energy exiting the control volume on the right side.

$$W_{pump} = \int_T (\dot{W}_{wall} - \dot{E}_{loss}) dt = \int_T (\dot{E}_{out} - \dot{E}_{in}) dt \quad (1.3)$$

#### 1.4.1 Principal of Operation

While there have been numerous experimental, computational, and analytical studies on the Liebau phenomenon, there have been only a few attempts at providing a full explanation for how net flow is generated in pumps based on the Liebau phenomenon. The first was Moser's impedance-defined flow, which attempted to explain how net flow can be generated in a closed loop using electrical impedance as a model for fluidic impedance (Moser et al., 1998). More recently, work from the Gharib research group at Caltech has provided substantial evidence for a wave resonance model that relies on partial

wave reflections from areas of mechanical wave impedance mismatch (Hickerson, 2005; Hickerson et al., 2005; Hickerson and Gharib, 2006; Rinderknecht et al., 2005; Rinderknecht, 2008; Forouhar, 2006; Loumes, 2007; Loumes et al., 2008; Avrahami and Gharib, 2008).

#### 1.4.1.1 Moser's Impedance-Defined Flow

Moser et al. (1998) proposed three necessary conditions for average flow around a closed loop to be generated based on the Liebau phenomenon. The three conditions below are taken verbatim from Moser et al. (1998) as they apply to the fluid and electric analog seen in Figure 1.6.

- **Condition One:** Energy must be provided to the system to move the fluid. If no energy is applied, no flow will occur. It turns out that the shape of the energy pulse is critical for the efficiency of the system. Short duration rapid ejection followed by a relatively long relaxation period, appears advantageous.
- **Condition Two:** The circuit must contain a compliant reservoir to allow for storage of the displaced fluid. If no compliant reservoir is available, no storage can occur, owing to the incompressibility of the fluid.
- **Condition Three:** The impedance in the two pathways,  $Z_1$  and  $Z_2$  of the system must be different and at least one of the two must be a complex number. If both are complex numbers, their phases must be different. Where this is not the case the displaced volume through either branch will be equal to the volume returned through that branch, and no average flow will occur. At the point of symmetry, both branches have equal impedance and no average flow can be observed.

Moser's hypothesis goes a long way in explaining how the Liebau phenomenon might generate a net flow, and explains many previous experimental observations such as the need for asymmetry and compliance in the system. However, many experimental observations are not explained by Moser's hypothesis, including frequency dependent flow reversals.

#### 1.4.1.2 Mechanical Wave Impedance and Resonance

Hickerson (2005) recognized that the wave dynamics in the compliant pumping region and the wave reflections at its ends, where a mechanical wave impedance mismatch occurs, play a critical role in determining the resonance conditions where high flow rates are observed. Mechanical waves generated from the pressure increase in the fluid filled compliant tubes propagate away from the excitation location and are partially reflected where the compliant tube is coupled to the flow loop

and the mechanical wave impedance changes. Figure 1.9 shows a schematic of a typical impedance pump with a compliant tube of impedance  $Z_o$ , coupled to tubing of different impedance.

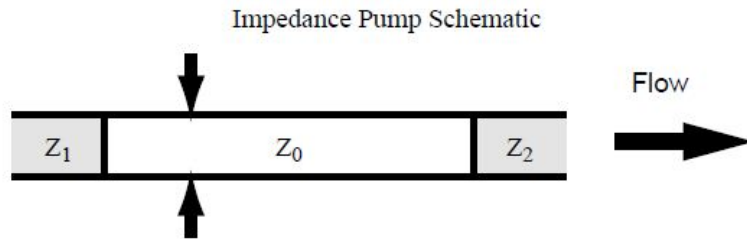


Figure 1.9: A schematic of an impedance pump, where the compliant tube has an impedance  $Z_o$  and is coupled at either end to rigid tubes with impedance  $Z_1$  and  $Z_2$ . Typically,  $Z_1 = Z_2$ , but the important condition for wave reflection in the pump is that  $Z_1$  and  $Z_2$  are different than  $Z_o$ .

Hickerson and Gharib (2006) showed that constructive interaction between generated and reflected waves were likely responsible for the resonant flow peaks seen in impedance pump flow behaviors using a simple 1-D wave pulse model to predict the frequencies of maximum flow seen in her experimental system. Avrahami and Gharib (2008) and Hickerson (2005) also found that resonant flow behavior was observed at frequencies defined by Equation 1.4, where  $c$  is the wave speed in the fluid filled compliant tube and  $L$  is the length of the compliant tube.

$$f_{res} = \frac{c}{2L} \quad (1.4)$$

#### 1.4.2 Liebau Phenomenon on the Microscale

Only a few studies have looked at the flow behavior of impedance pumps on the size scale relevant to microfluidic, biomedical, and medical devices applications (Rinderknecht et al., 2005; Forouhar et al., 2006). Rinderknecht et al. (2005) and Rinderknecht (2008) used elastic tubes of 1.9 mm inner diameter and 250  $\mu\text{m}$  inner diameter to fabricate two different functional impedance pumps, but focused primarily on the electromagnetic actuation scheme used for the proposed devices. Rinderknecht provides one flow rate vs. frequency plot for the 1.9 mm diameter pump. The flow behavior shows resonance behaviors, and is consistent with the observations made during the extensive experimental study presented in this thesis. Rinderknecht (2008) also fabricated several prototype micro impedance pumps in both planar and tube based geometries seen in Figure 1.10.

As described in the motivation, valveless pumps based on the Liebau phenomenon show great promise for many microfluidic and medical applications. While the behaviors of the pumps on this size scale have not been studied extensively until now, several researchers have investigated

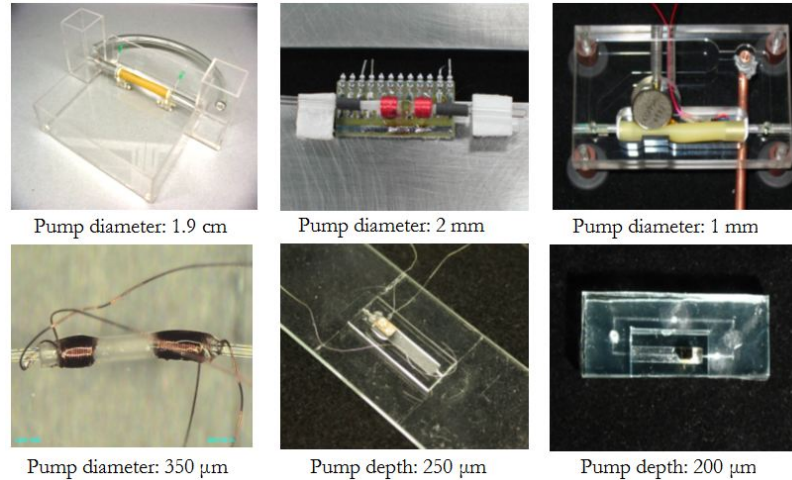


Figure 1.10: Top left shows the experimental setup of Hickerson (2005) and going clockwise are five micropump prototypes from Rinderknecht (2008) including a 2 mm electromagnetically actuated pump, 1 mm electromechanically actuated pump, a 200  $\mu\text{m}$  electromagnetically actuated planar pump, a 250  $\mu\text{m}$  piezoelectrically actuated planar pump, and a 350  $\mu\text{m}$  electromagnetically actuated pump. Images courtesy of Anna Hickerson and Derek Rinderknecht.

methods for manufacturing such devices. Chang et al. (2007), Lee et al. (2008), Yeo et al. (2008), and Wang et al. (2010) have all proposed methods of fabricating planar impedance pump based devices actuated by both piezoelectric discs and electromagnetic actuation similar to Rinderknecht et al. (2005). This thesis provides the experimental data and analysis necessary to understand the behaviors of the Liebau phenomenon at the relevant size scales and enable the development of practical impedance-pump-based microfluidic devices.

## 1.5 Thesis Objectives

Rinderknecht et al. (2005) showed that the Liebau phenomenon successfully scales to the microscale, but it is not known what effect various excitation and system parameters might have on the performance of such pumps. It is clear from the literature survey that there is likely more than one simple mechanism responsible for the broad phenomenon of valveless pumping. In one scenario, Moser's proposed directionally dependent dynamic resistance might play the major role in rectifying the flow in a preferred direction. However, under another operating condition the energy transfer between the passive portion of the pump and the working fluid might be more important in developing the large resonant flow responses seen in the studies of Hickerson (2005) and Avrahami and Gharib (2008). These two mechanisms, curiously relying on different definitions of the concept of impedance, play greater or lesser roles in the development of a net flow depending on the scaling of important parameters in valveless pump systems. The parameters in Table 1.1 will play a critical

role in predicting the performance and behavior of valveless microscale pumps.

<b>Excitation</b>	Spatial Parameters	Amplitude
		Location
		Width
		Shape
	Temporal Parameters	Offset
		Frequency
Duty Cycle		
<b>Pumping Element</b>	Geometric Parameters	Wave form
		Length
		Cross-sectional Area
		Aspect Ratio
	Material Parameters	Thickness
		Elastic Modulus
		Storage Modulus
		Loss Modulus
<b>System/Loop</b>	Working Fluid Parameters	Compliance
		Density
	Material and Geometric Parameters	Viscosity
		Resistance
		Symmetry
		Compliance
Overpressure		

Table 1.1: Impedance pump parameter space

The main objective of this thesis is to develop an understanding of the major mechanisms responsible for valveless pumping on small size scales. This objective will be achieved through a carefully verified experimental characterization and systematic exploration of the parameter space described in Table 1.1. Table 1.1 is not meant to be an exhaustive list of parameters that play a role in valveless pumping behavior, nor is it practical to attempt to investigate all of these parameters in a single experimental thesis.

When extending a previously studied phenomenon to a new size scale, it is important to consider the scaling behavior. Two important scaling parameters to consider for the oscillatory flow in valveless pumping are Reynolds number, Equation 1.5 and Womersley number, Equation 1.6. The flows seen in the experimental study of Hickerson (2005) with a 1.9 cm I.D. pump had a maximum Reynolds number of  $Re \approx 6700$  and maximum Womersley number of  $\alpha \approx 30$ . Comparatively, the maximum Reynolds number seen in the current study is  $Re \approx 132$  and the maximum Womersley number is  $\alpha \approx 20$ .

$$Re_d = \frac{\rho U d}{\mu} \quad (1.5)$$

$$\alpha = r \sqrt{\frac{2\pi f \rho}{\mu}} \quad (1.6)$$

The drop in Reynolds number is clearly a function of the decreased size scales and flow velocities for smaller scale impedance pumps. However, the relative preservation of the Womersley number arises from the fact that many excitation parameters, including frequency, will scale linearly with the pump size scale for a given material and elastic modulus. The excitation amplitude and width can be expected to scale linearly with the decreasing lengths and diameters of a given pump. One length scale that can be expected to deviate from this scaling behavior is the wall thickness of the pump. As the pump is scaled down, at some point the wall thickness must stop decreasing as fast, and the ratio of wall thickness to pump length will increase. If the wall thickness were to continue decreasing, at some point it would become too fragile for practical use. This relative increase in wall thickness will lead to a relative increase in wave speed in the system, thus affecting the resonant frequencies where resonant flow behaviors are expected.

In the study presented in this thesis, the thin-walled tubes relatively preserve the scaling of the wall thickness to the pump length compared to Hickerson (2005), 0.0025 for this study compared to 0.0017 for Hickerson (2005). However, the thick-walled tubes deviate by an order of magnitude, with a wall thickness to pump length ratio of 0.0125. A consequence of this relative increase in wall thickness, is a decrease in compliance and therefore an increase in wave speed. In fact, for the thick-walled pumps, the wave speed in the pumping element is approximately 50 m/s, placing the resonant frequency as defined by Hickerson (2005) an order of magnitude out of reach of the characterization system used for this study. However, the thick-walled pumps not only still function at frequencies an order of magnitude below their expected resonant frequency, they show higher volumetric efficiencies than the thin-walled pumps. This unexpected behavior is further evidence that the flow rectification mechanism for valveless pumping based on the Liebau phenomenon is not fully understood.

Through exploration of various pump, loop, and fluid properties, this thesis will answer important questions for designing practical impedance pump based devices on the microscale and hopefully illuminate important scaling behaviors that increase our understanding of the Liebau phenomenon. Each of the following questions will be answered in Chapter 5 based on the experimental results of this study.

- Which behaviors previously observed on large scale impedance pumps scale down to microscale valveless pumps?

- Which parameters from Table 1.1 are most important in determining the performance of a valveless pump?
- What level of prediction of pump direction at different frequencies can be achieved?
- What effect will increased fluid density and viscosity have on microscale valveless pump performance?
- How do the dynamics of planar valveless pumps differ from tube-based pumps?
- What are the most important parameters to consider when designing a microscale system or device utilizing a valveless pump?
- Can a valveless pump be treated as a stand-alone device, or is its fundamental behavior always a function of the system it operates on?
- What can be said about the efficiency of valveless pumps beyond the volumetric efficiency approach of previous literature?
- What different flow regimes exist as outputs of valveless pumps? Can a periodically excited valveless pump put out a steady flow rate?
- What are the transient behaviors of small scale valveless pumps, and what are the implications for practical devices?

## Bibliography

- D. Auerbach, W. Moehring, and M. Moser. An analytic approach to the Liebau problem of valveless pumping. *Cardiovascular Engineering*, 4(2):201–207, 2004.
- I. Avrahami and M. Gharib. Computational studies of resonance wave pumping in compliant tubes. *Journal of Fluid Mechanics*, 608:139–160, 2008.
- C. F. Babbs. Behavior of a viscoelastic valveless pump: a simple theory with experimental validation. *Biomedical Engineering Online*, 9, 2010.
- A. Borzi and G. Propst. Numerical investigation of the Liebau phenomenon. *Zeitschrift Fur Angewandte Mathematik Und Physik*, 54(6):1050–1072, 2003.
- H. J. Bredow. An avalvular flow principle derived from human circulation. *Klinische Wochenschrift*, 46(15):840, 1968.
- T. T. Bringley, S. Childress, N. Vandenberghe, and J. Zhang. An experimental investigation and a simple model of a valveless pump. *Physics of Fluids*, 20(3), 2008.
- H. T. Chang, C. Y. Lee, and C. Y. Wen. Design and modeling of electromagnetic actuator in mems-based valveless impedance pump. *Microsystem Technologies — Micro-and Nanosystems-Information Storage and Processing Systems*, 13(11–12):1615–1622, 2007.
- A. S. Forouhar. *Dynamic views of structure and function during heart morphogenesis*. PhD thesis, Caltech, 2006.
- A. S. Forouhar, M. Liebling, A. Hickerson, A. Nasiraei-Moghaddam, H. J. Tsai, J. R. Hove, S. E. Fraser, M. E. Dickinson, and M. Gharib. The embryonic vertebrate heart tube is a dynamic suction pump. *Science*, 312(5774):751–753, 2006.
- A. I. Hickerson. *An Experimental Analysis of the Characteristic Behaviors of an Impedance Pump*. PhD thesis, Caltech, 2005.
- A. I. Hickerson and M. Gharib. On the resonance of a pliant tube as a mechanism for valveless pumping. *Journal of Fluid Mechanics*, 555:141–148, 2006.
- A. I. Hickerson, D. Rinderknecht, and M. Gharib. Experimental study of the behavior of a valveless impedance pump. *Experiments in Fluids*, 38(4):534–540, 2005.
- E. Jung, S. Lim, W. Lee, and S. Lee. Computational models of valveless pumping using the immersed boundary method. *Computer Methods in Applied Mechanics and Engineering*, 197(25–28):2329–2339, 2008.

- E. N. Jung and C. S. Peskin. Two-dimensional simulations of valveless pumping using the immersed boundary method. *Siam Journal on Scientific Computing*, 23(1):19–45, 2001.
- I. J. Karassik. *Pump handbook*. McGraw-Hill, New York, 2nd edition, 1986.
- T. Kenner, M. Moser, I. Tanev, and K. Ono. The Liebau-effect or on the optimal use of energy for the circulation of blood. *Scripta Medica*, 73(1):6, 2000.
- D. J. Laser and J. G. Santiago. A review of micropumps. *Journal of Micromechanics and Microengineering*, 14(6):R35–R64, 2004.
- C. Y. Lee, H. T. Chang, and C. Y. Wen. A mems-based valveless impedance pump utilizing electromagnetic actuation. *Journal of Micromechanics and Microengineering*, 18(3), 2008.
- S. Lee and E. Jung. A two-chamber model of valveless pumping using the immersed boundary method. *Applied Mathematics and Computation*, 206(2, Sp. Iss. SI):876–884, 2008.
- W. Lee, E. Jung, and S. Lee. Simulations of valveless pumping in an open elastic tube. *Siam Journal on Scientific Computing*, 31(3):1901–1925, 2009.
- L. B. Leverett, J. D. Hellums, C. P. Alfrey, and E. C. Lynch. Red blood cell damage by shear stress. *Biophys J*, 12:257–273, 1972.
- G. Liebau. Arterielle pulsation und venose repulsation (arterial pulsation and venous repulsation). *Zeitschrift Fur Die Gesamte Experimentelle Medizin Einschliesslich Experimenteller Chirurgie*, 123(1):71–90, 1954a.
- G. Liebau. Uber ein ventillosoes pumpprinzip (about a valveless pump system). *Naturwissenschaften*, 41(14):327–327, 1954b.
- G. Liebau. Die stromumngsprinzipien des herzens (the flow principles of the heart). *Zeitschrift Fur Kreislaufforschung*, pages 677–684, 1955a.
- G. Liebau. Prinzipien kombinierter ventilloser pumpen, abgeleitet vom menschlichen blutkreislauf (principles of combined valveless pumps, derived from human blood circulation). *Naturwissenschaften*, 42(11):339, 1955b.
- G. Liebau. Die bedeutung der tragheitskrafte fur die dynamic des blutkreislaufs (the importance of inertial forces for the dynamic circulation of the blood). *Zeitschrift Fur Kreislaufforschung*, pages 428–438, 1956.
- G. Liebau. Uber die funktionelle bedeutung der venenklappen. *Zeitschrift Fur Kreislaufforschung*, 52(4):419, 1963.

- S. Lim and E. Jung. Three-dimensional simulations of a closed valveless pump system immersed in a viscous fluid. *Siam Journal on Applied Mathematics*, 70(6):1999–2022, 2010.
- L. Loumes. *Multilayer Impedance Pump: A Bio-inspired Valveless Pump with Medical Applications*. PhD thesis, Caltech, 2007.
- L. Loumes, I. Avrahami, and M. Gharib. Resonant pumping in a multilayer impedance pump. *Physics of Fluids*, 20(2), 2008.
- J. Maenner, A. Wessel, and T. M. Yelbuz. How does the tubular embryonic heart work? looking for the physical mechanism generating unidirectional blood flow in the valveless embryonic heart tube. *Developmental Dynamics*, 239(4):1035–1046, 2010.
- O. Mahrenholtz. Ein beitrag zum forderprinzip periodisch arbeitender, ventiloser pumpen (a contribution to first principles of periodic, valveless pumps). *Forschung im Ingenieurwesen*, 20(2): 47–56, 1963.
- C. G. Manopoulos, D. S. Mathioulakis, and S. G. Tsangaris. One-dimensional model of valveless pumping in a closed loop and a numerical solution. *Physics of Fluids*, 18(1), 2006.
- M. Moser, J. W. Huang, G. S. Schwarz, T. Kenner, and A. Noordergraaf. Impedance defined flow: generalization of William Harvey’s concept of the circulation — 370 years later. *International Journal of Cardiovascular Medicine and Science*, 1(3/4):205–211, 1998.
- M. Nabavi. Steady and unsteady flow analysis in microdiffusers and micropumps: a critical review. *Microfluidics and Nanofluidics*, 7(5):599–619, 2009.
- A. Olsson, P. Enoksson, G. Stemme, and E. Stemme. Micromachined flat-walled valveless diffuser pumps. *Journal of Microelectromechanical Systems*, 6(2):161–166, 1997.
- J. T. Ottesen. Valveless pumping in a fluid-filled closed elastic tube-system: one-dimensional theory with experimental validation. *Journal of Mathematical Biology*, 46(4):309–332, 2003.
- G. Propst. Pumping effects in models of periodically forced flow configurations. *Physica D — Nonlinear Phenomena*, 217(2):193–201, 2006.
- H. J. Rath and I. Teipel. Pumping effect in valveless elastic tubes. *Zeitschrift Fur Angewandte Mathematik Und Physik*, 29(1):123–133, 1978.
- D. Rinderknecht. *Development of a microimpedance pump for pulsatile flow transport - Part 1 : Flow characteristics of the microimpedance pump. Part 2: A systematic study of steady and pulsatile transport in microscale cavities*. PhD thesis, Caltech, 2008.

- D. Rinderknecht, A. I. Hickerson, and M. Gharib. A valveless micro impedance pump driven by electromagnetic actuation. *Journal of Micromechanics and Microengineering*, 15(4):861–866, 2005.
- M. Rosenfeld and I. Avrahami. Net flow rate generation by a multi-pincher impedance pump. *Computers and Fluids*, 39(9):1634–1643, 2010.
- S. J. Shin and H. J. Sung. Three-dimensional simulation of a valveless pump. *International Journal of Heat and Fluid Flow*, 31(5, Sp. Iss. SI):942–951, 2010.
- S. Takagi and T. Saijo. On a pipe-capacity-system with a t-junction .1. study of a piston pump without valves. *Bulletin of the Japan Society of Mechanical Engineers*, 26(218):1366–1372, 1983.
- S. Takagi and K. Takahashi. Study of a piston pump without valves .2. pumping effect and resonance in a pipe-capacity-system with a t-junction. *Bulletin of the Japan Society of Mechanical Engineers*, 28(239):831–836, 1985.
- H. Thomann. Simple pumping mechanism in a valveless tube. *Zeitschrift Fur Angewandte Mathematik Und Physik*, 29(2):169–177, 1978.
- S. Timmermann and J. T. Ottesen. Novel characteristics of valveless pumping. *Physics of Fluids*, 21(5), 2009.
- C.-C. Wang. *Effects of actuator impact on the nonlinear dynamics of a valveless pumping system*. PhD thesis, National Cheng Kung University, 2011.
- Y. H. Wang, Y. W. Tsai, C. H. Tsai, C. Y. Lee, and L. M. Fu. Design and analysis of impedance pumps utilizing electromagnetic actuation. *Sensors*, 10(4):4040–4052, 2010.
- C. Y. Yeo, W. K. Shim, E. Wouterson, T. Li, and J. Ma. Piezoelectric materials for impedance driven micro-channel flow. *Functionnl Materials Letters*, 1(3):225–228, 2008.

## Chapter 2

# Experimental Methods and Materials

### 2.1 Experimental Objectives

A main objective of this experimental study is to obtain detailed, dynamic pressure and flow data during the operation of a variety of small scale impedance pumps for a large range of operating parameters. The parameters chosen for investigation in this thesis include a range of excitation locations, amplitudes, offsets, and frequencies. The characterization loop will also allow us to look at the effects of increased transmural pressure, variable fluid viscosity and density, and variable loop resistance. During all of these studies we want the ability to look at dynamic and average flow and pressure behaviors in both transient and steady state operation.

To achieve these objectives, a valveless pump characterization system was carefully designed to facilitate a parametric study based on the properties outlined above. The characterization system was designed to facilitate simple swapping of different pumping elements of both tube and planar geometries like these described in Section 2.3.1 and Section 2.3.2.

### 2.2 Characterization System

A pump placed in the characterization system can be excited at any point along its length with a resolution of 0.01 mm. The tip of the excitation probe is a half cylinder with diameter,  $d = 2.8$  mm, and length,  $l = 8$  mm. The excitation profile is sinusoidal with an amplitude and offset resolution of approximately 0.05 mm. Dynamic pressure data was captured at both the inlet and the exit of the pump, and dynamic flow rate data was measured in the middle of the flow loop. The flow loop was designed with two prime/purge valves to easily fill and evacuate the loop with different working

fluids, as well as rid the loop of air bubbles. Great care was taken to ensure the flow loop was symmetric. Loop properties such as fluidic resistance and volumetric compliance were measured and are discussed below.

Figure 2.1 shows all of the major components of the characterization system. The pump is excited by a steel excitation probe attached to a BK Type 4810 Mini-Shaker linear actuator. A Sentech 75DC-125 Linear Variable Differential Transformer is used to track the position of the excitation probe. Two Omega PX26-001 flow through pressure transducers are used to monitor the dynamic differential pressure across the impedance pump. A Transonic Systems TS410 Tubing Module with ME2PXN111 Flow Meter is used to measure the flow rate in the system. The data acquisition system consists of a National Instruments PCI-6035E DAQ, National Instruments BNC connector block, and a series of custom MATLAB scripts written to control the motion of the excitation probe and capture the desired data.

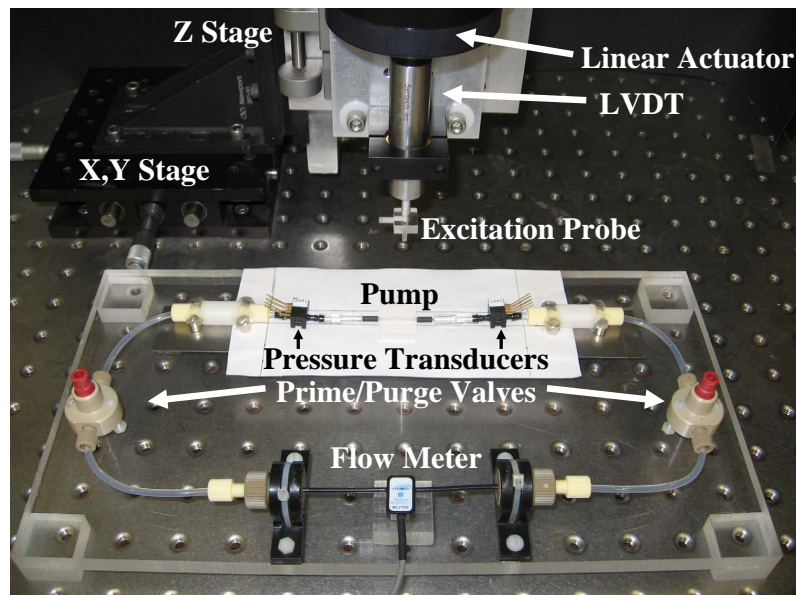


Figure 2.1: Experimental characterization system

### 2.2.1 Loop Resistance

One primary objective of this study is to obtain a standard pumping curve, spanning low resistance (high flow rate) to infinite resistance (no flow rate), for a variety of valveless pumps in order to better understand the flow generation mechanisms. In addition to the original flow loop described above, three extra lengths of tubing are available to add to the loop to increase the flow resistance.

The loop can also be completely occluded. This provides for five distinct values of loop resistance,  $K$ , which were measured using steady flow from a syringe pump and recorded in Table 2.1.

Loop	$K$ [kPa] / [mL/min]
Original	0.14
Resistance #1	0.24
Resistance #2	0.30
Resistance #3	0.45
Occluded	Infinite

Table 2.1: Loop resistance measurements

### 2.2.2 Equipment Specifications

Sensor	Range	Published Accuracy	Response Time	Typical Signal:Noise Amplitude
Pressure	$\pm 6.9$ kPa	0.069 kPa	1 ms (3rd Order Butterworth Filter with 160Hz Cutoff)	1000:1
Flow	$\pm 50$ mL/min	$\pm 0.02$ mL/min *(Resolution at 10Hz)	3rd Order Butterworth Filter with 160Hz Cutoff	4:1
LVDT	$\pm 2.97$ mm	0.015mm	-3dB at 500 Hz	80:1
NI-DAQ	$\pm 5$ V	.005 V	$f_{sample} = 5000$ Hz	-

Table 2.2: Sensor specifications

<b>BK Mini-Shaker - Type 4810</b>	
Force Rating	10N (2.25 lbs) sine peak
Frequency Range	DC to 18 kHz
Maximum Bare Table Acceleration	550 $m/s^2$
Maximum input current	1.8 A
Maximum DC displacement	6 mm

Table 2.3: Linear actuator specifications

### 2.2.3 Data Acquisition and Filtering

The DAQ is a NI PCI-6035E with 16 single ended or 8 differential analog input channels. For the majority of the experiments, 4 differential analog input channels were used (LVDT, Flow, Pressure Transducer #1, and Pressure Transducer #2), as well as 1 analog output (to amplifier driving the BK voicecoil).

One unique aspect of this study was the ability to get high resolution dynamic information related to the pressure and flow output of the impedance pump. However, because our DAQ was not capable of simultaneous sampling between channels, it was necessary to characterize the time lag between input channels in order to perform a reliable time-based comparison of dynamic information from the input channels. More information on characterizing the performance of the data acquisition system can be found in Appendix A.

The Transonic TS410 flow meter does not have an option for unfiltered output data, and the highest cutoff frequency allowed is a 160 Hz 3rd-order Butterworth filter. Fortunately, this filter is complementary with the dynamic range of the BK voicecoil at the amplitudes and loads under investigation. To solve a problem of high output impedance and low signal output, the pressure transducers were passed through a KH Model 3988 preamp and given a 10 dB output gain before being filtered with a 160 Hz 3rd-order Butterworth filter in MATLAB for consistency with the flow data. The filter's effect on the phase and magnitude of the signal are represented below by the Bode plot shown in Figure 2.2. The effect of excitation frequency was measured for a range of 0–140 Hz. The BK voicecoil reaches its dynamic force limit near 140 Hz with the extra weight from the excitation probe and the excitation amplitudes under consideration. The mandatory 160 Hz 3rd-order Butterworth filter also decreases the magnitude of dynamic signals to a value of 0.83 of its original value at 140 Hz. It should also be noted that the filter causes a significant phase shift in the dynamic data at these high frequencies, which must be taken into account when analyzing the dynamic behaviors of the pump.

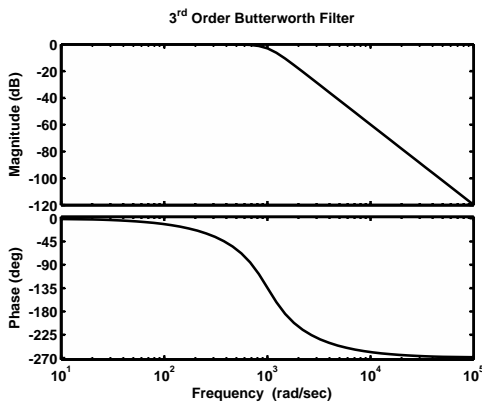


Figure 2.2: The effect of a 3rd-order Butterworth filter with a 160 Hz (1005.3 rad/s) cutoff frequency on the gain and phase of frequency content in sampled data

## 2.3 Material Properties

### 2.3.1 Tube-Based Pumps

Glass capillaries were cut into 20 mm lengths and the ends were filed and rounded to prevent sharp edges that might puncture the thin-walled tubes. Tygon tubing with a 1/16" inner diameter and 1/16" walls was cut into 15 mm lengths to serve as the connection between the glass capillaries and the tubing barbs on the pressure transducers. The Tygon tubing was thick enough to be assumed rigid compared to the much higher compliance found in all pumping elements tested. 1/8" heat shrink tubing was used to seal the pumping element to the glass capillaries. Figure 2.3 below shows a selection of completed pumps. All tubular pumps were fabricated in this fashion.

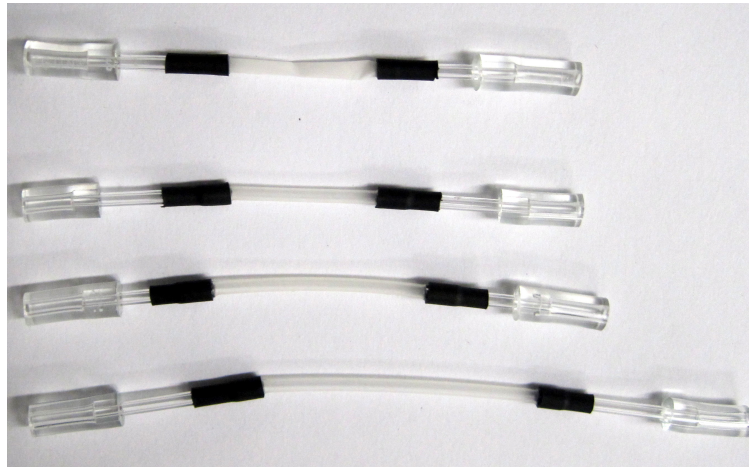


Figure 2.3: Tube-based pumps prepared for the characterization system

#### 2.3.1.1 Elastic Modulus Measurements

For a tube of radius  $r$  much greater than its wall thickness  $t$ , experiencing a transmural pressure  $P$ , the hoop stress can be determined by Equation 2.1.

$$\sigma_{\theta} = \frac{Pr}{t} \quad (2.1)$$

Every tube used in this study was filled with water and pressurized to a series of known pressures spanning the range of dynamic pressures seen during experiments. The diameter change was monitored and recorded under a microscope. The strain in the tube walls ( $\frac{\Delta r}{r}$ ) was measured from the calibrated images and related back to the inferred hoop stress from Equation 2.1 using Equation 2.2.

$$\sigma_{\theta} = E \frac{\Delta r}{r} \quad (2.2)$$

The measured values of elastic modulus for every pump used in this study can be found in Table 2.4. These elastic modulus values are valid for 0–10% strain in the tube wall.

### 2.3.2 Planar Sheet Pumps

As mentioned in the introduction, it is more practical for real devices to utilize planar versions of the impedance pump, both for ease of fabrication and matching the form factor of current LOC and biomedical devices. A planar pump frame was designed to achieve a similar pump volume as found in the tubular pumps. The pump frame was designed to sandwich thin sheets of silicone and seal the pumping cavity. The fabrication of the planar pump frame was performed by the Caltech Aeronautics Machine Shop. Three silicone membranes of identical thickness ( $250 \mu\text{m}$ ) were obtained from LGS Technologies BISCO Silicones with varying elastic modulus. The membranes were cut into 24 mm x 23 mm squares that were then able to be sandwiched in the planar pump frame. Figure 2.4 below shows the dimensions and final fabricated version of the planar pump frame.

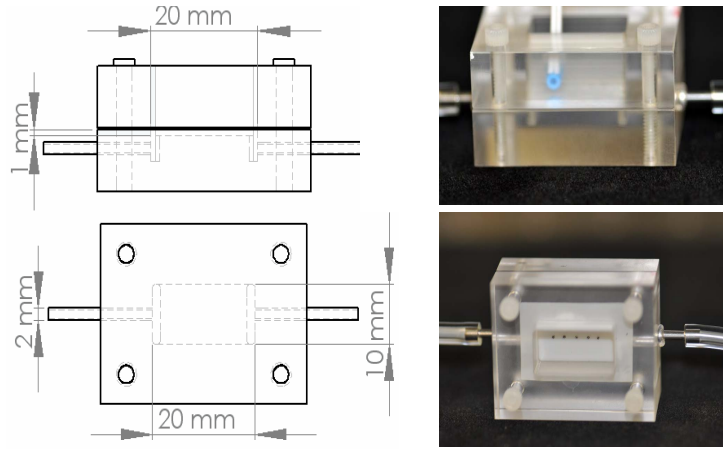


Figure 2.4: Planar pump frame with dimensioned schematic

#### 2.3.2.1 Elastic Modulus Measurements

The elastic modulus of each of the three planar silicone membranes was measured with the help of Christopher Kovalchick of Dr. Ravichandran’s lab by measuring the force required to elongate rectangular samples of the silicone membranes through a range of known displacements. The data series and linear fit to determine the elastic modulus for strains up to 8% can be seen in Figure 2.5.

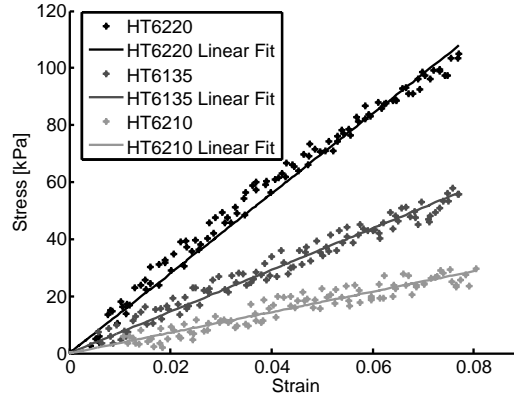


Figure 2.5: Elastic modulus measurements of planar elastic membranes. HT6135/White ( $E = 1.4$  MPa), HT6220/Black ( $E = 0.73$  MPa), HT6210/Grey ( $E = 0.36$  MPa)

### 2.3.3 Pumping Element and Loop Compliance

One of the important system parameters identified in Table 1.1 is the compliance of the pumping element, and potentially more importantly the relative compliance of the pumping element to the compliance of the flow loop. Hickerson (2005) defined the compliance of a tube as  $C = \frac{\partial A / \partial P}{A_0}$ . To relate more intuitively to the characterization system, and really to any flow loop or real world pumping environment that will have various geometries and tube diameters throughout, it is better to define compliance as  $C = \frac{\partial V / \partial P}{V_0}$ . However, if one assumes that the pumping element length is constant and the increase in radius is constant across the length of the tube, the two compliance definitions are actually equivalent.

The compliance of each pumping element was measured by filling the element with water, assumed incompressible. The pressure was then monitored as the volume of water in the pumping element was increased by known amounts, effectively increasing the volume of the pumping element. The compliance of the flow loop was measured in the same manner to determine the relative compliance of the pumping elements to the loop itself. Table 2.4 summarizes the properties and results of all elastic modulus and compliance tests for every pumping element used in this study.

<b>Form Factor</b>	<b>Name</b>	<b>Manufacturer Model #</b>	<b>I.D. [mm]</b>	<b>Wall Thickness [mm]</b>	<b>E [MPa]</b>	<b>Pump Length [mm]</b>	<b>Compliance [1/MPa]</b>
Tube	ABThick-2cm	AB PAT06	1.5	0.25	13.5	20	3-8
Tube	ABThick-3cm	AB PAT06	1.5	0.25	13.5	30	2-5
Tube	ABThick-4cm	AB PAT06	1.5	0.25	13.5	40	3-6
Tube	DOW006-2cm	Dow Silastic 508-006	1.47	0.24	11.4	20	3-8
Tube	Latex Thin	Custom HT-201	1.8	0.05	1.0	20	45-74
Sheet	White-Stiff	Bisco Silicone HT6135	1.5	0.25	1.4	20x10	89-90
Sheet	Black-Medium	Bisco Silicone HT6220	1.5	0.25	0.73	20x10	166-169
Sheet	Grey-Soft	Bisco Silicone HT6210	1.5	0.25	0.36	20x10	337-339
Tube	Flow Loop	-	-	-	-	750	.7 - 1.2

Table 2.4: Pumping element and flow loop properties

## Bibliography

- A. I. Hickerson. *An Experimental Analysis of the Characteristic Behaviors of an Impedance Pump*.  
PhD thesis, Caltech, 2005.

## Chapter 3

# Experimental Results

### 3.1 Basic Behaviors

The characterization system described in Chapter 2 produced an expansive data set of valveless pumping behaviors under various conditions. In this chapter, the reader can systematically step through some of those results for thin-walled tubes, thick-walled tubes, and planar pumps. More detailed analysis of the data will follow in Chapter 4.

To facilitate the comprehension of the large quantity of data, Figure 3.1 below shows a schematic representation and definition of each parameter that can be varied in the following tests.

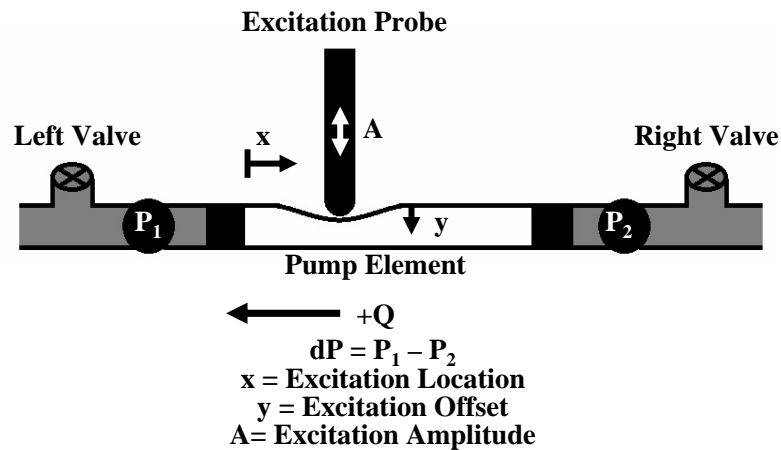


Figure 3.1: Schematic of a general test in the characterization system show system variable definitions. The valves shown act to open the loop to atmospheric pressure or allow a water column to be placed on the loop to increase the transmural pressure. Flow freely moves around the loop whether these valves are open or closed.

Table 3.1 summarizes the results presented in this chapter, following the wave speed and resonant frequency measurement results.

Pump	Results Presented
Thin Latex Tube	Flow rate vs. frequency (0-140 Hz) Flow rate vs. excitation location (5-15 mm) Flow rate vs. excitation amplitude (.3-.55 mm) Flow rate vs. excitation offset (.8-1.2 mm) Flow rate vs. pressure venting conditions Flow rate vs. transmural pressure (0.46-1.37 kPa) Flow rate vs. loop resistance (0.14 kPa/(mL/min) - infinity) Flow rate vs. viscosity (0.95-28.23 mPa*s)
Thick AB Tube	Flow rate vs. frequency (0-140 Hz) Flow rate vs. pump length (2-4 cm) Flow rate vs. excitation location (5-15 mm) Flow rate vs. excitation amplitude (.3-.45 mm) Flow rate vs. excitation offset (.8-1.2 mm) Flow rate vs. pressure venting conditions Flow rate vs. transmural pressure (0.39-1.52 kPa) Flow rate vs. loop resistance (0.14 kPa/(mL/min) - infinity) Flow rate vs. viscosity (0.95-28.23 mPa*s)
Planar Silicone	Flow rate vs. frequency (0-140 Hz) Flow rate vs. excitation location (5-15 mm) Flow rate vs. pressure venting Flow rate vs. elastic modulus (.36-1.4 MPa) Flow rate vs. viscosity (0.95-8.9 mPa*s)

Table 3.1: Results presented in this chapter

### 3.1.1 Wave Speed

In Section 2.3, each pumping element was carefully characterized by measuring its compliance and elastic modulus. The elastic modulus is thought to be a critical parameter in determining the behavior of valveless pumps based on the Liebau phenomenon, because it plays a strong role in determining the wave speed in the fluid-filled elastic tube. Hickerson (2005) developed a wave pulse model based on the wave speeds in her pumping element that correctly predicted maximum flow peaks at a resonant frequency defined as  $f_{res} = c/2L$ , where  $L$  is the total length of the pump and  $c$  is the Moens-Korteweg wave speed, Equation 3.1. The Moens-Korteweg wave speed is the propagation velocity for a pressure disturbance in a thin-walled elastic tube of diameter  $d$ , elastic modulus  $E$ , and wall thickness  $h \ll d$ , filled with an incompressible fluid of density  $\rho$ . The result comes from solving the axisymmetric Navier-Stokes equations for a thin-walled linear elastic tube filled with an incompressible fluid. The amplitude of the propagating pressure disturbance should also be much smaller than the diameter of the tube, while the wavelength of the disturbance should be much greater than the diameter. For a detailed derivation see Zamir (2000).

$$c = \sqrt{\frac{Eh}{\rho d}} \quad (3.1)$$

The Moens-Korteweg approximation for wave speed in a fluid-filled elastic tube is relevant for

all of the tubes used in this thesis and the expected wave speed was calculated from known and measured properties. The theoretical wave speeds were also verified through careful measurement of the phase lag between the pressure pulses reaching the transducers on either side of the pump after a single high frequency compression. Figure 3.2 illustrates this concept.

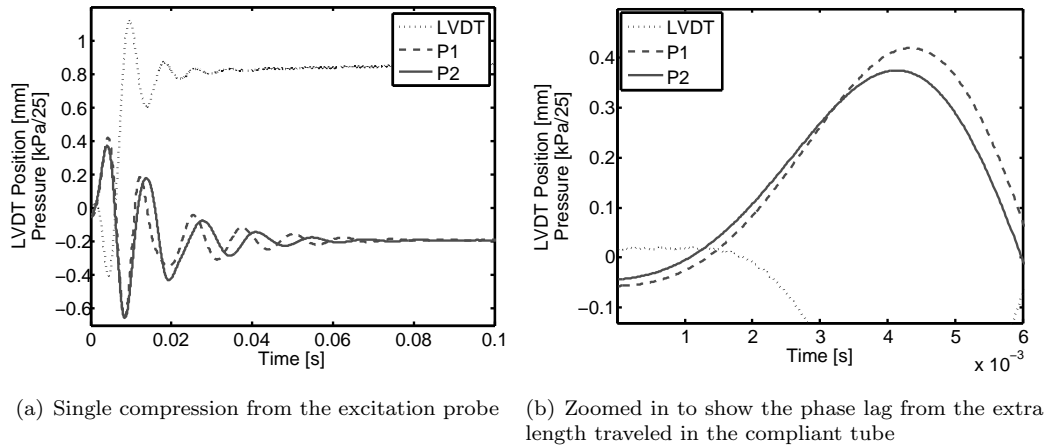


Figure 3.2: Example of phase lag between the two pressure transducers due to a finite and measurable wave speed in the fluid filled elastic tube

The pressure disturbance generated at the point of impact of the excitation probe travels in both directions away from the probe at a finite wave speed, approximately the Moens-Korteweg wave speed, through the fluid-filled elastic pump element. This pressure disturbance then propagates into the rigid loop at the speed of sound in water, approximately 1500 m/s (assuming a rigid flow loop), and is measured by the pressure transducers on either side of the pumping element. If the excitation takes place asymmetric with respect to the length of the pumping element, the pressure measured at the transducer further from the excitation will lag behind the transducer closer to the excitation. If two measurements are performed in this way at different, but known, locations along the length of the tube, the difference between the two measured phase lags can be used to calculate the actual disturbance propagation velocity in the fluid-filled elastic tube. By using two points, the unknown disturbance propagation velocity in the flow loop and any other systematic unknowns, such as the precise response time of the pressure transducers can be removed from the measurement. The limiting factor that determines the resolution with which the propagation velocities in the tube can be determined is then the switching time of the multiplexer in the data acquisition system. This value was experimentally determined to be approximately 1/50,000 Hz or 20  $\mu$ s for the experiments performed, which is consistent with the use of four input channels and a maximum sample rate of 200,000Hz for all channels. The result of the phase lag measurements performed at two excitation locations a known distance  $\Delta x$  apart, with phase lags of  $\Delta t_1$  and  $\Delta t_2$  can be used to calculate the wave propagation velocity in the fluid-filled elastic pumping element using Equation 3.2.

$$c = \frac{2\Delta x}{\Delta t_2 - \Delta t_1} \quad (3.2)$$

The results of both the calculated Moens-Korteweg wave speed and the measured wave speed are summarized in Table 3.2 along with measured damped natural frequency of the pumping elements placed in the flow loop. There is good agreement between the calculated Moens-Korteweg wave speed and the measured wave speed of a pressure pulse in the tube.

### 3.1.2 Resonant Frequency

Previous studies have also commented on the importance of the damped natural frequency of the system, which does not necessarily match the resonant frequency defined by Hickerson (2005). Hickerson (2005) defined the resonant frequency as the wave speed in the tube divided by two times the pump length, but this does not take into account the mass of fluid in the closed loop which should have an effect on the damped natural frequency of the system. A simple method of measuring the damped natural frequency is to perturb the pressure in the system with a step input and observe the freely oscillating response. Takagi and Takahashi (1985) used this method to determine the damped natural frequency of a rigid T-junction pumping system and found that the performance of the valveless pump was maximum with opposite sign on either side of this resonant frequency, passing through zero flow rate at the resonant frequency. A similar perturbation method was used in this study and the measured damped natural frequencies are recorded along with the measured and calculated wave speeds in Table 3.2. The pressure perturbation was generated with an impulsive strike of the pumping element.

<b>Form Factor</b>	<b>Name</b>	<b>E [MPa]</b>	<b>Pump Length [mm]</b>	<b>Compliance [1/MPa]</b>	<b>Moens-Korteweg [m/s]</b>	<b>Measured c [m/s]</b>	<b>Measured <math>f_{res}</math> [Hz]</b>
Tube	ABThick-2cm	13.5	20	3-8	47.4	44-58	81-84
Tube	ABThick-3cm	13.5	30	2-5	47.4	43-53	75-78
Tube	ABThick-4cm	13.5	40	3-6	47.4	42-50	74-76
Tube	DOW006-2cm	11.4	20	3-8	43.1	59-77	77-80
Tube	Latex Thin	1.0	20	45-74	5.27	4.7-4.8	94-98
Sheet	White-Stiff	1.4	20x10	89-90	-	2.8	149-159
Sheet	Black-Medium	0.73	20x10	166-169	-	2.8	148-157
Sheet	Grey-Soft	0.36	20x10	337-339	-	2.3	143-152
Tube	Flow Loop	-	750	.7 - 1.2	-	-	-

Table 3.2: Summary of wave speed and resonant frequency measurements. Values with a range represent the uncertainty in the measurement due to the limited resolution of the DAQ timing.

### 3.2 Thin-Walled Tube as a Pump

The standard method of viewing valveless pump performance is to look at the steady-state mean flow response as a function of the excitation frequency. For each set of parameters explored below, the pump was excited at a frequency of 1 Hz and then 5 Hz–140 Hz in 5 Hz increments for a total of 29 unique excitation frequencies. Almost every distinct set of parameters was also run more than once, so the data presented is an average of all tests with errorbars representing the range of values seen in all tests. The full list of experimental parameters defined in Figure 3.1 will be stated in the caption of each plot shown below. Typical excitation conditions were  $x = 5$  mm,  $y = 1$  mm, and  $A = 0.4$  mm.

Figure 3.3 shows an example data set of mean pressure and flow data taken from the excitation of a thin-walled tube. The average pressure and flow were calculated from dynamic measurements sampled at 5000 Hz and filtered with the previously described filters. Some clearly recognizable features of the pump performance are the first resonant flow peak at 60 Hz in this case, the flow reversal at 95 Hz and the negative flow peak at 130 Hz. Figure 3.3(c) shows the mean differential pressure plotted against the mean flow rate for a constant loop resistance of approximately 0.17 kPa/(mL/min).

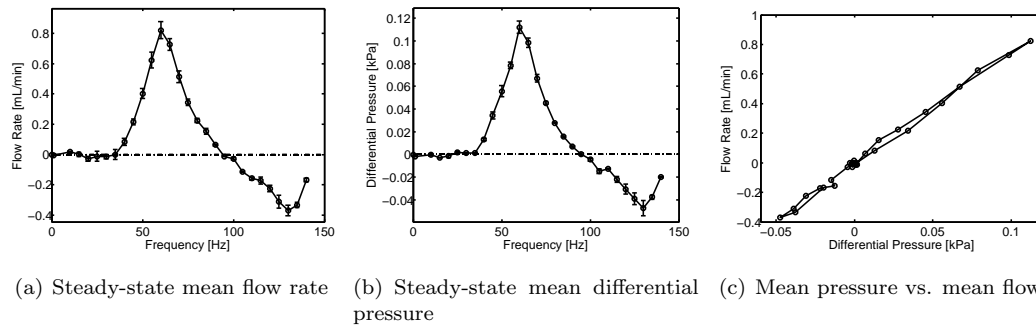


Figure 3.3: Example data set from the excitation of the Latex Thin tube. ( $x = 5$  mm,  $y = 1$  mm,  $A = 0.4$  mm, valves = right valve open with .45 kPa water column)

### 3.2.1 Excitation Location

In Figure 3.4, the reader can observe several behaviors similar to those seen in the larger scale impedance pump studies of Hickerson (2005). The pump behavior is relatively symmetric around the midpoint along the length of the pump, with the direction of flow switching sign as the excitation location switches sides of the pump. As the excitation location becomes more asymmetric, the flow rate increases. There is also a slight shift of the frequency at which maximum flow is achieved, suggesting that the relative length of pump tubing on each side of the actuation plays an important role in determining the apparent resonant behavior of the flow. It should be noted that the frequency of maximum flow decreases as excitation location becomes more symmetric, but the point of flow reversal appears to be independent of excitation location.

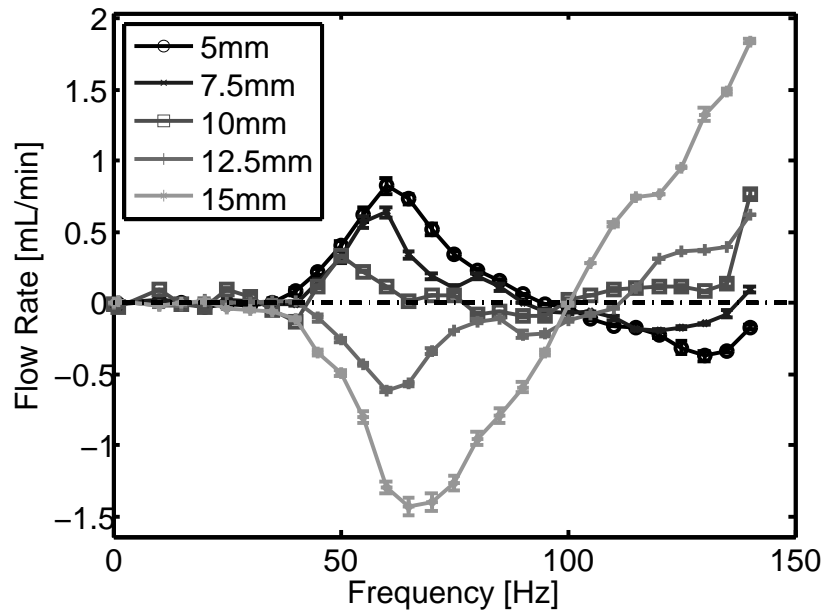
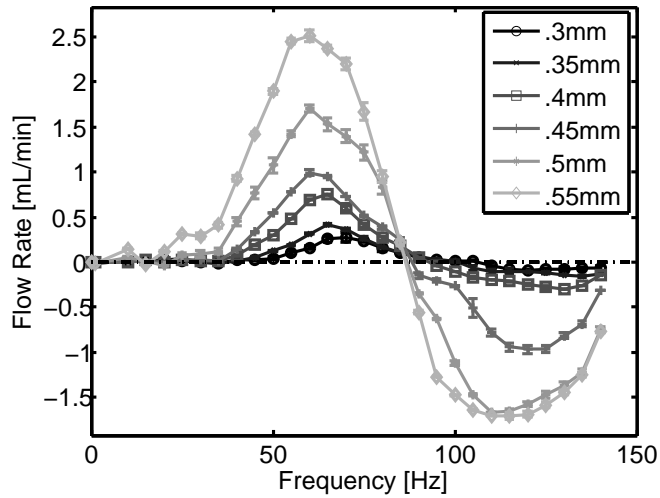


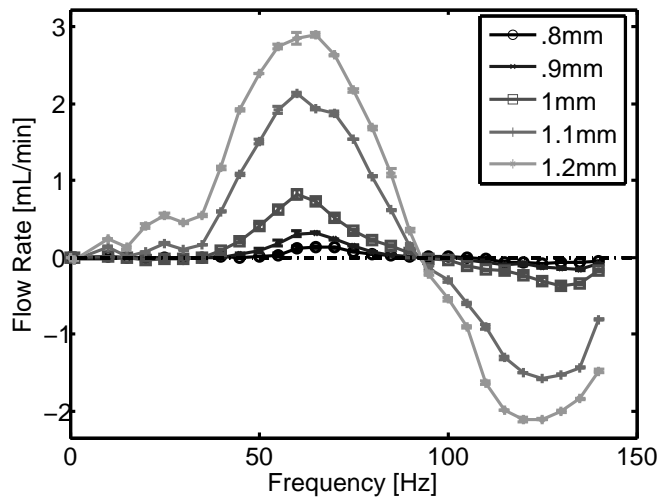
Figure 3.4: Latex Thin tube performance as a function of excitation location. ( $y = 1$  mm,  $A = 0.4$  mm, valves = right valve open with .45 kPa water column)

### 3.2.2 Excitation Amplitude and Offset

Figure 3.5 shows that changing the amplitude and offset of the excitation have similar effects. The performance follows the intuitive behavior that the more volume the pincher displaces, the greater the flow rate. The amplitude and offset of the excitation appear to have little or no effect on the frequency of flow reversal, but there may be a slight decrease in the maximum flow frequency as the amplitude and offset are increased.



(a) Variable excitation amplitude



(b) Variable excitation offset

Figure 3.5: Latex Thin tube performance as a function of excitation amplitude and offset. ( $x = 5$  mm,  $y = 1$  mm and variable,  $A = 0.4$  mm and variable, valves = right valve open with .45 kPa water column)

### 3.2.3 Inlet/Outlet Pressure Condition (Venting)

Venting one side of the loop or the other to atmosphere has little effect on the behavior of the thin-walled pump. Venting the flow loop to atmosphere essentially drives the compliance of the flow loop to infinity. This switch in compliance has a much more dramatic effect in the thick-walled pump cases. There is a slight shift in the maximum flow frequency and magnitude of maximum flow, but this is likely related to transmural pressure effects discussed later. The thin-walled tube is very sensitive to changes in transmural pressure which change the tension in the tube wall.

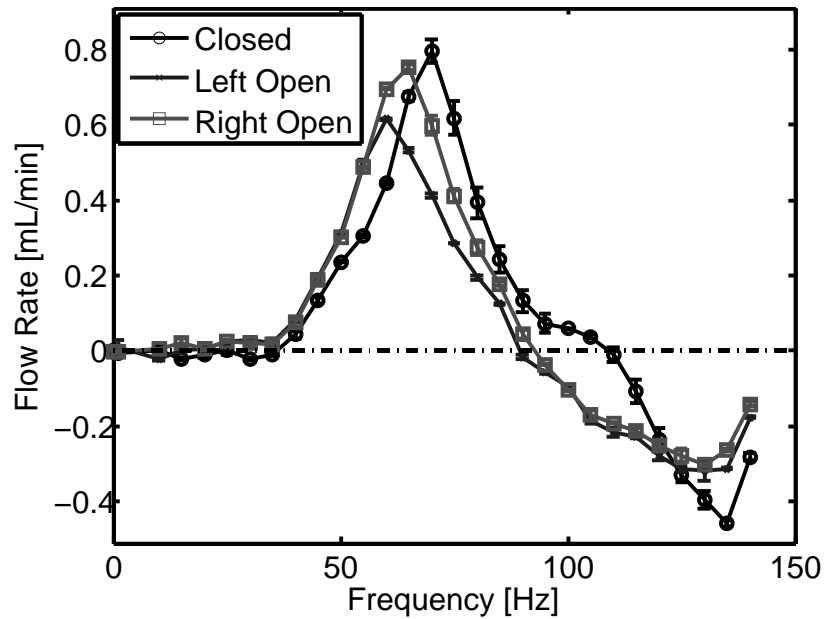


Figure 3.6: Latex Thin tube performance as a function of inlet pressure conditions. ( $x = 5$  mm,  $y = 1$  mm,  $A = 0.4$  mm)

### 3.2.4 Transmural Pressure

Increasing the transmural pressure will increase the hoop stress and the tension in the tube wall. From the elastic modulus measurements on the thin-walled tube, it is known that a transmural pressure of 1.37 kPa will create a strain of approximately 2%. This increased strain and wall tension is the likely cause for the increase in frequency of maximum flow. We might expect the frequency of maximum flow to scale with the square root of the wall tension, similar to the scaling of the wave speed and resonant frequency of a rope in tension.

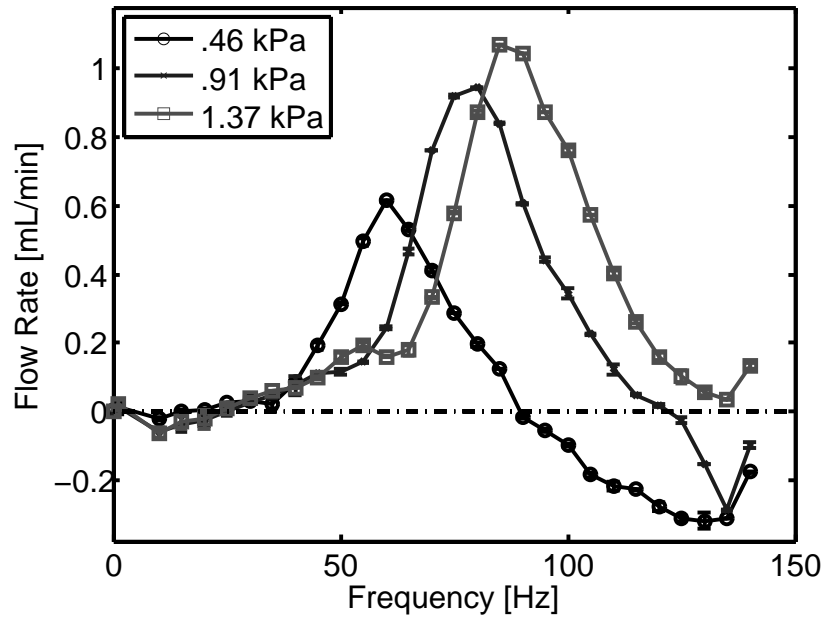
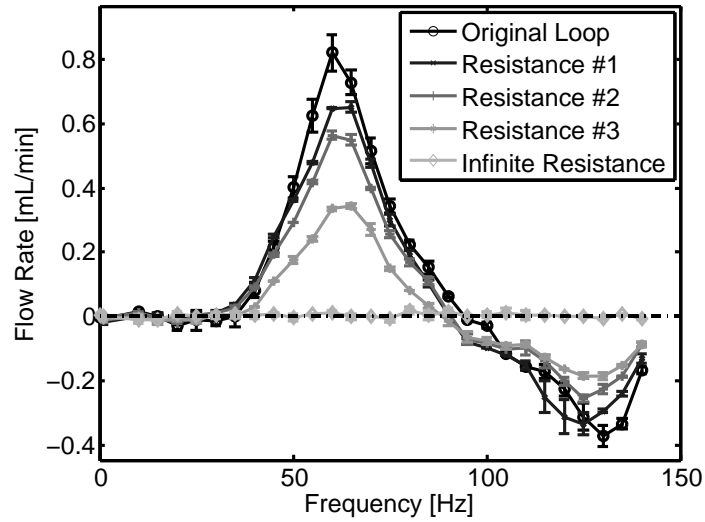


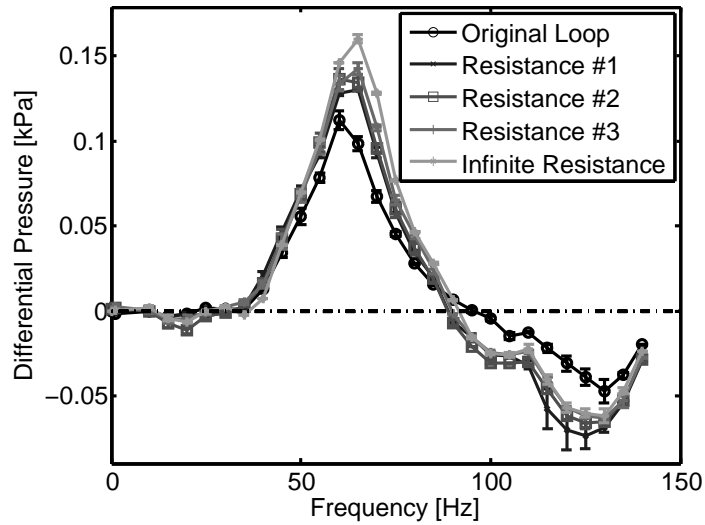
Figure 3.7: Latex Thin tube performance as a function transmural pressure. ( $x = 5$  mm,  $y = 1$  mm,  $A = 0.4$  mm, valves = left valve open with various water columns)

### 3.2.5 Loop Resistance

As the reader would expect for a black box pump, the flow rate goes down and the differential pressure increases as the loop resistance increases. There is little change in the other relevant system behaviors to changes in loop resistance.



(a) Mean flow rate

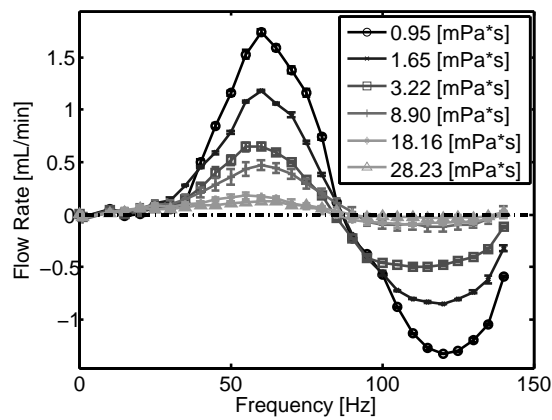


(b) Mean differential pressure

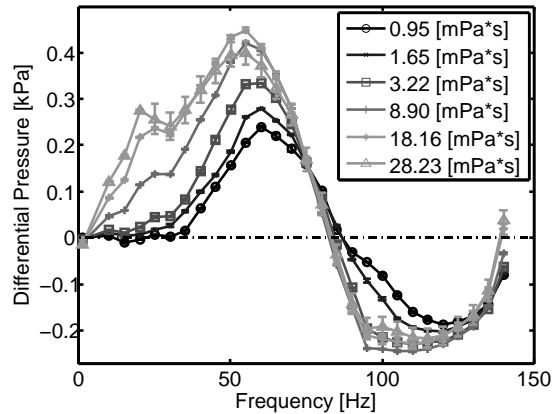
Figure 3.8: Latex Thin tube performance as a function of loop resistance. ( $x = 5$  mm,  $y = 1$  mm,  $A = 0.4$  mm, valves = right valve open with .45 kPa water column)

### 3.2.6 Viscosity Effects

As the viscosity of the working fluid increases, we see behaviors similar to the increased loop resistance. However, the pump appears to produce a greater differential pressure, likely due to the slight increase in density of the glycerine based working fluids. There also appears to be a slight decrease in the frequency at which maximum differential pressure is achieved. If we make the rope in tension analogy again, we would expect the wave speed and thus the resonant frequency to scale as the square root of the inverse of the density. This analogy is in qualitative agreement with the results. For a detailed characterization of the glycerine based viscosity standards used in this study, see Appendix B.



(a) Mean flow rate



(b) Mean differential pressure

Figure 3.9: Latex Thin tube performance as a function of fluid viscosity. ( $x = 5$  mm,  $y = 1$  mm,  $A = 0.5$  mm, valves = right valve open with .45 kPa fluid column)

### 3.3 Thick-Walled Tube as a Pump

In contrast to the thin-walled tube studies, there were two different thick-walled tubes from different manufacturers with slightly differently properties. Results from both tubes will be presented for comparison where relevant. Pump length was also introduced as a variable in the thick-walled studies.

#### 3.3.1 Excitation Location and Tube Length

The behaviors of the thick-walled tubes were harder to isolate, likely because they had compliance (2-8 1/MPa) on the same order as the flow loop (0.7-1.2 1/MPa). The implications of the compliance similarity are discussed in Chapter 4. Figure 3.10 shows that changing the overall length of the pump does have a significant effect on the performance, but it is difficult to isolate behaviors of the pump from the flow loop for the thick-walled tube.

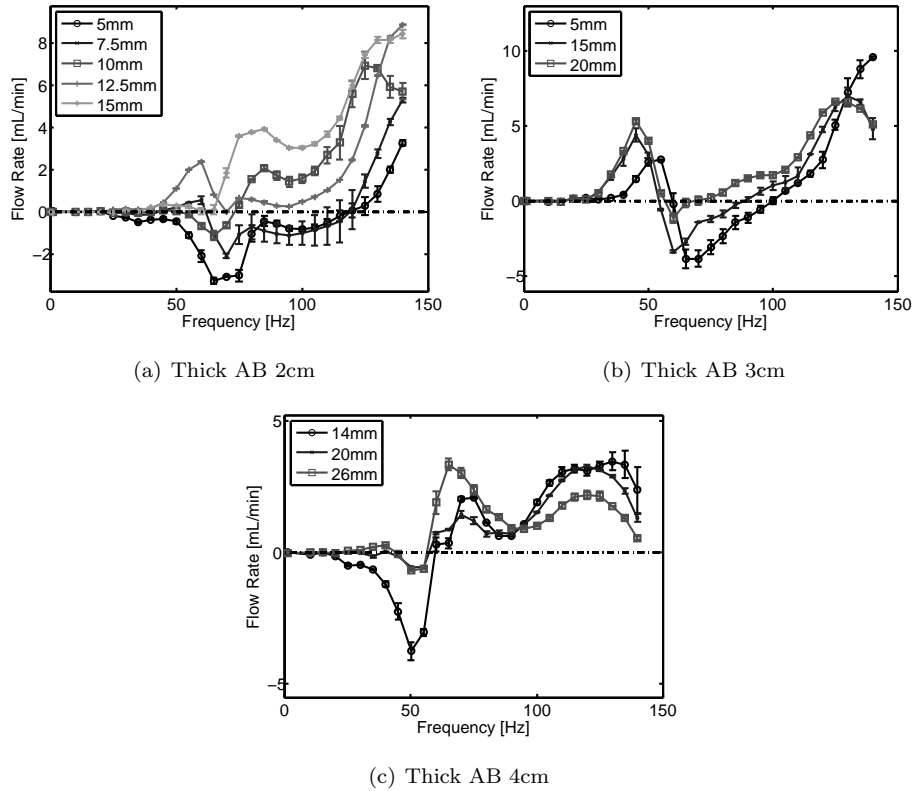


Figure 3.10: ABThick-2cm, ABThick-3cm, and ABThick-4cm tubing excited at various positions. (x = variable, y = 1 mm, A = 0.4 mm, valves = closed)

It can be seen in Figure 3.11 that if both sides of the flow loop are opened, essentially driving its compliance to infinity, the symmetry about the length of the pump returns.

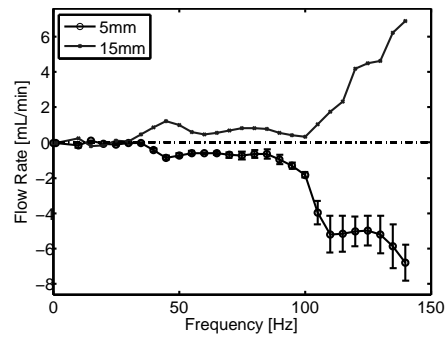
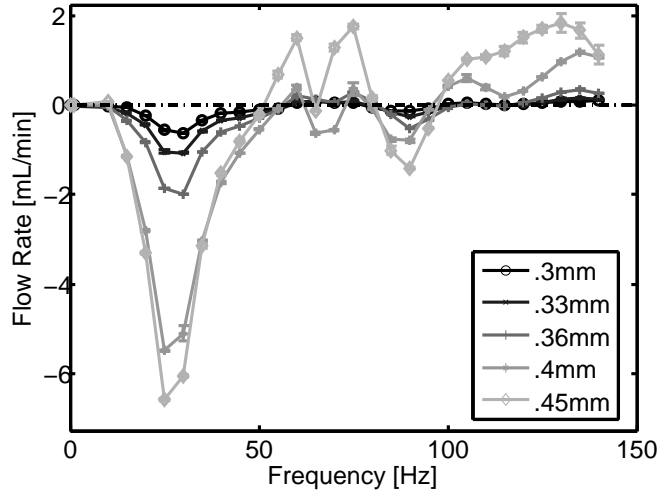


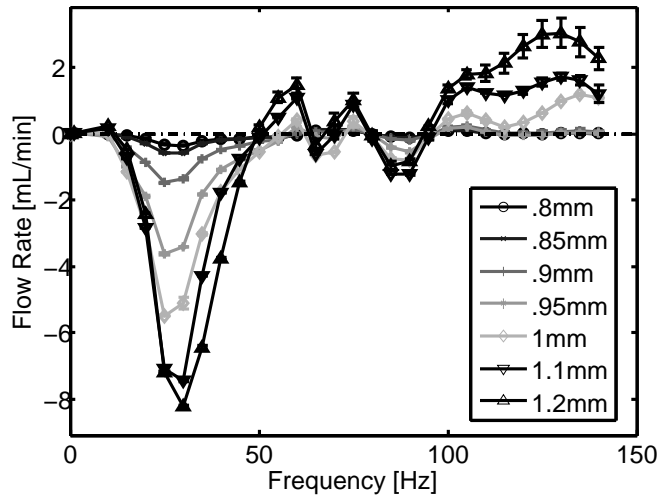
Figure 3.11: DOW006-2cm tubing excited at various positions. ( $x$  = variable,  $y = 1.1$  mm,  $A = 0.4$  mm, valves = both open)

### 3.3.2 Excitation Amplitude and Offset

Excitation amplitude and offset have the same consequences in the thick-walled tubes as they did for the thin-walled tubes.



(a) Variable excitation amplitude



(b) Variable excitation offset

Figure 3.12: ABThick-2cm tube performance as a function of excitation amplitude and offset. ( $x = 5$  mm,  $y = 1$  mm and variable,  $A = 0.4$  mm and variable, valves = closed)

### 3.3.3 Inlet/Outlet Pressure Condition (Venting)

The compliance similarities between the pump and the flow loop lead to some interesting behaviors when one side or the other of the flow loop is vented to atmosphere, essentially driving its compliance to infinity. Figure 3.13 and Figure 3.14 show that symmetric, opposite flow behaviors occur when the left side of the loop is vented compared to when the right side of the loop is vented. The venting is essentially another way to introduce asymmetry since the loop and the pump appear to have coupled dynamics in the thick-walled cases.

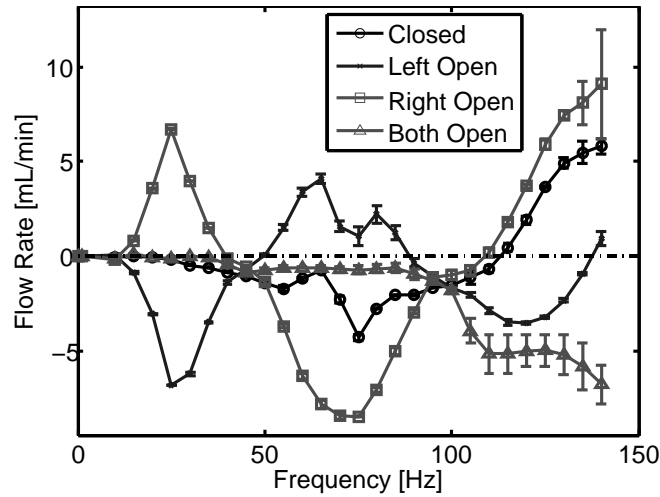


Figure 3.13: DOW006-2cm tube performance as a function of variable inlet and outlet pressure conditions ( $x = 5$  mm,  $y = 1.1$  mm,  $A = 0.4$  mm, valves = variable)

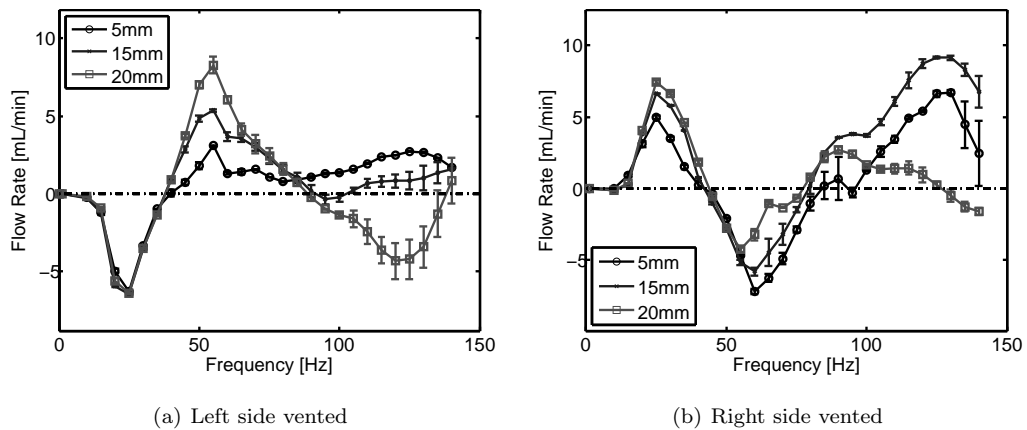


Figure 3.14: ABThick-3cm tube performance as a function of variable inlet and outlet pressure conditions and excitation position ( $x =$  variable,  $y = 1$  mm,  $A = 0.4$  mm, valves = variable)

### 3.3.4 Transmural Pressure

Changing the transmural pressure by up to 1.52 kPa has essentially no effect on the behavior of the thick-walled pumps. Transmural pressures of this magnitude create negligible strain or tension in the thick-walled pumps compared to the thin-walled pumps.

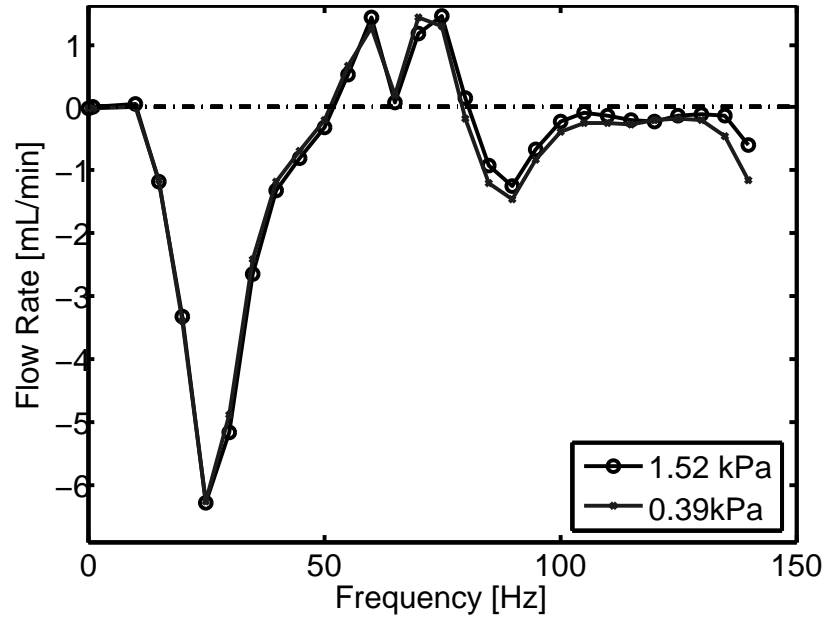
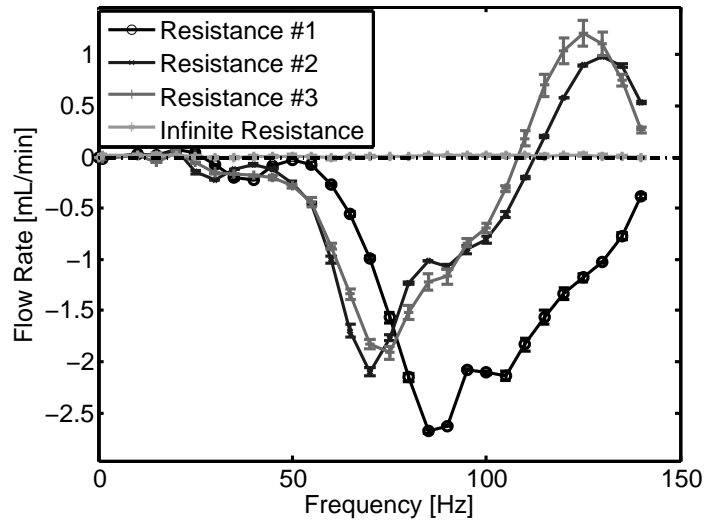


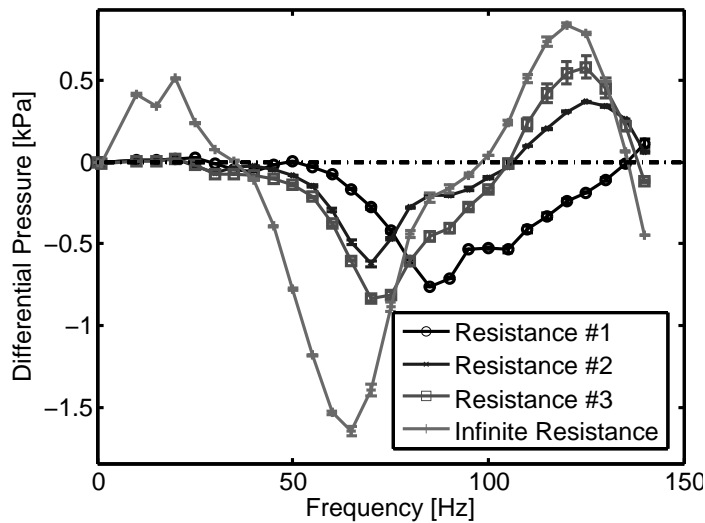
Figure 3.15: ABThick-2cm tube performance as a function of transmural pressure ( $x = 5$  mm,  $y = 1$  mm,  $A = 0.4$  mm, valves = left open with variable water column)

### 3.3.5 Loop Resistance

Increasing the loop resistance again decreases the flow rate and increases the differential pressure, however the dynamics are complicated by the fact that the pump and the flow loop are acting as one large, coupled, dynamic, pumping system.



(a) Mean flow rate

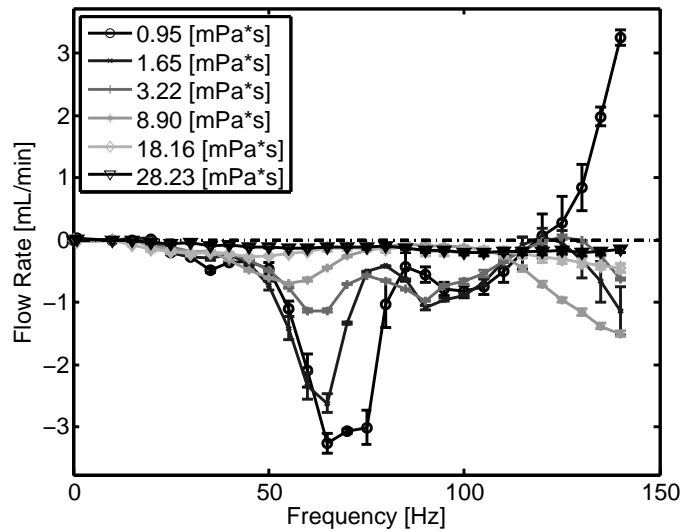


(b) Mean differential pressure

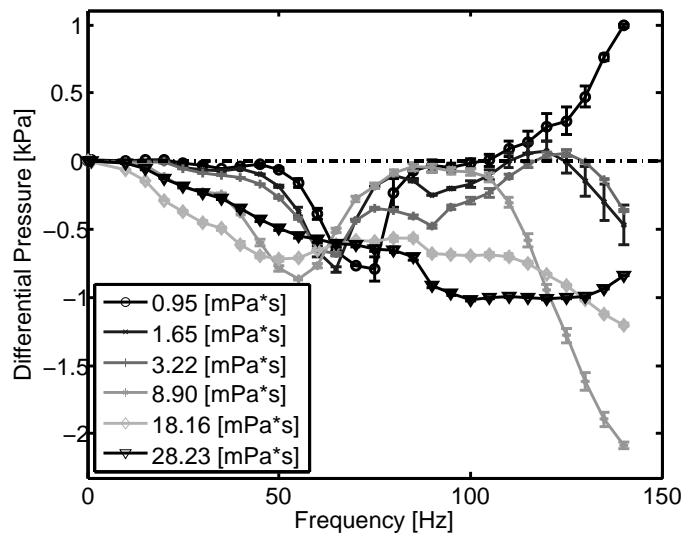
Figure 3.16: ABThick-2cm tube performance as a function of loop resistance. ( $x = 5$  mm,  $y = 1$  mm,  $A = 0.4$  mm, valves = closed)

### 3.3.6 Viscosity Effects

Figure 3.17 shows some behaviors similar to the thin-walled pumps. The flow rate decreases with increasing viscosity and the frequency at which maximum flow is achieved decreases with increasing fluid density. However, the differential pressure generated at a resonant flow peak does not appear to increase with increasing fluid density, and the high frequency flow response changes dramatically as the fluid viscosity/density changes.



(a) Mean flow rate



(b) Mean differential pressure

Figure 3.17: ABThick-2cm tube performance as a function of fluid viscosity. ( $x = 5$  mm,  $y = 1$  mm,  $A = 0.4$  mm, valves = closed)

## 3.4 Planar Pumps

### 3.4.1 Excitation Location

The planar pumps had the lowest measured compliance of any of the pumping elements, so they are expected to behave more like the thin-walled tubes than the thick-walled tubes. Figure 3.18 shows a partially symmetric behavior about the length of the pump, particularly with no flow being generated when the pump is excited at its midpoint. However, the results of excitation 5 mm from the right end and 5 mm from the left end are not exactly inverses of each other. It is not known for certain what causes this behavior, but possible explanations include trapped bubbles which were much more problematic and difficult to flush out in the planar pump experiments or uneven clamping of the pump membrane.

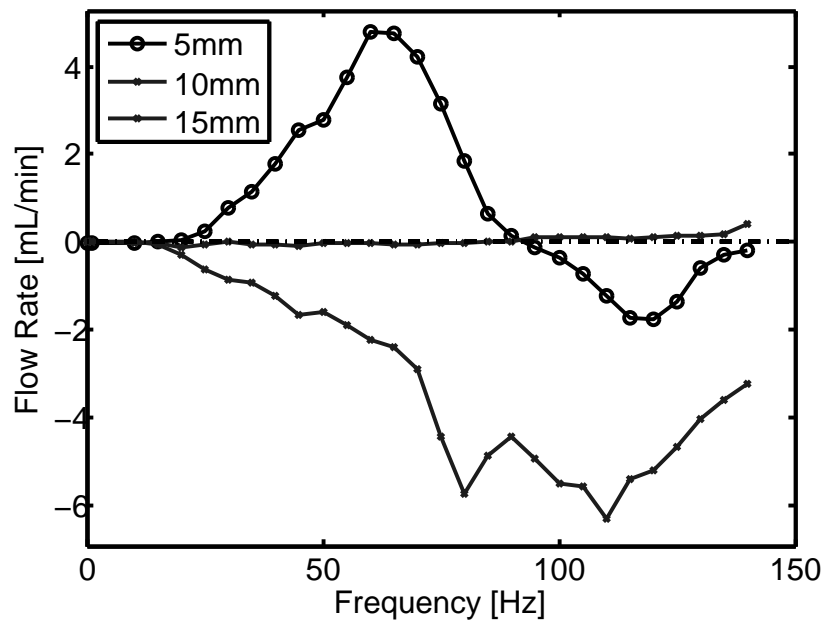


Figure 3.18: Planar White-Stiff membrane (1.4 MPa) performance as a function of excitation location ( $x$  = variable,  $y$  = .5 mm,  $A$  = 0.4 mm, valves = closed)

### 3.4.2 Inlet/Outlet Pressure Condition (Venting)

Similar to the thin-walled pumps, changing the venting conditions to the left or right side of the pump did not fundamentally change the behavior of the pump. Figure 3.19 does show a slight shift in the frequency of peak flow and a decreased performance for frequencies between 100 Hz to 120 Hz for the right vent open compared to the left vent open. However, these behaviors should be compared to the thick-walled studies where the direction of flow at the resonant flow peak actually changes directions when the venting conditions are changed. The small changes in behavior seen in Figure 3.19 could be a result of some small dependence on the compliance of the loop for the planar pumps, but the changes in behavior are relatively minor and considered insignificant compared to the flow direction change seen in the thick-walled cases.

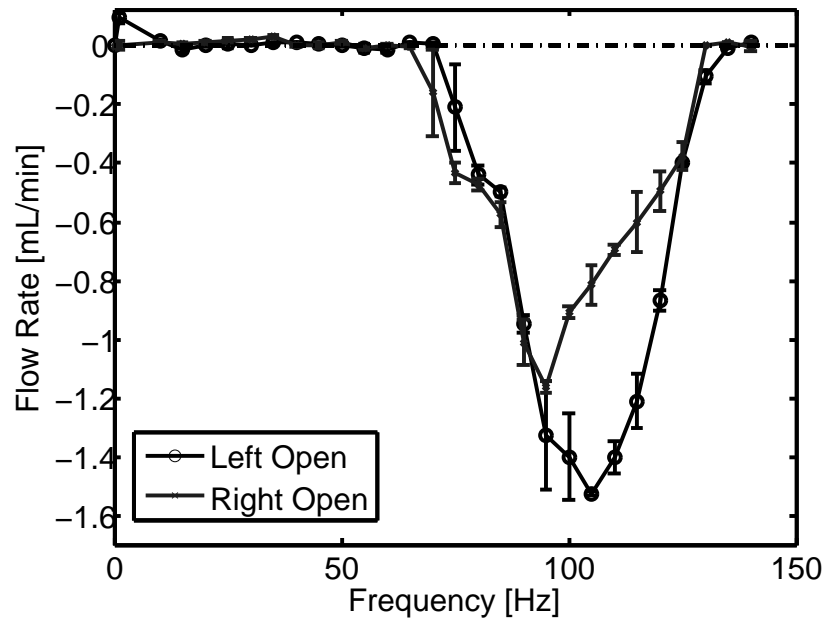


Figure 3.19: Planar White-Stiff membrane (1.4 MPa) performance as a function of variable inlet and outlet pressure conditions ( $x = 5$  mm,  $y = .5$  mm,  $A = 0.4$  mm, valves = variable)

### 3.4.3 Elastic Modulus Effects

As the elastic modulus of the pumping element increased, the resonant flow frequency and the magnitude of the flow at resonance increased. The increase in resonant frequency is qualitatively consistent with an expected increase in wave speed scaling with the elastic modulus of the membrane. If we assume similar wave propagation to a tube based pump and that the bulging mode pressure wave is a key driver of the resonant response then we would expect the resonant frequency to scale with the square root of the elastic modulus, based on the Moens-Korteweg wave speed. However, the shift in resonant frequency is less than what would be expected for Moens-Korteweg, potentially due to geometric effects from the planar geometry or suggesting that a different resonant phenomenon is at play.

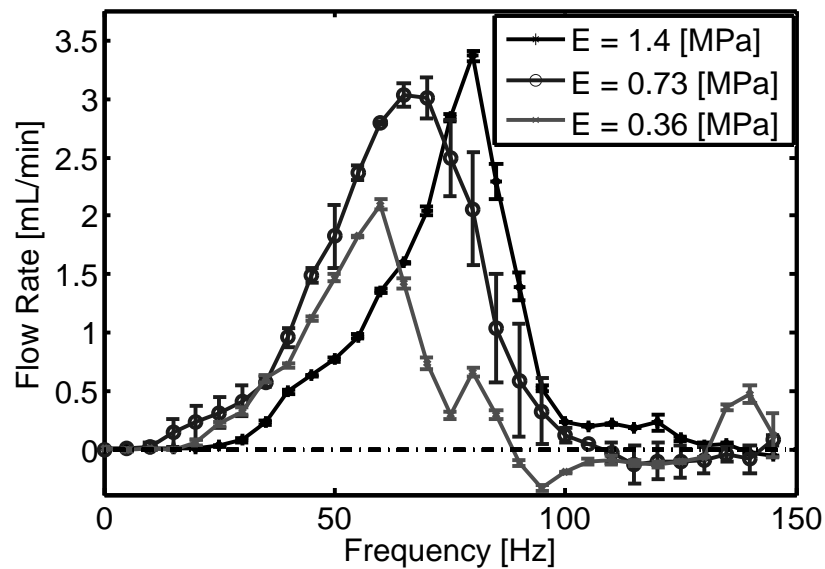


Figure 3.20: Planar pump performance as a function of variable membrane elastic modulus ( $x = 5$  mm,  $y = .5$  mm,  $A = 0.4$  mm, valves = closed)

### 3.4.4 Viscosity Effects

Figure 3.21 again shows behaviors similar to the thin-walled pumps. The flow rate decreases with increasing viscosity (and density) and the frequency that maximum flow is achieved decreases with increasing fluid density (and viscosity).

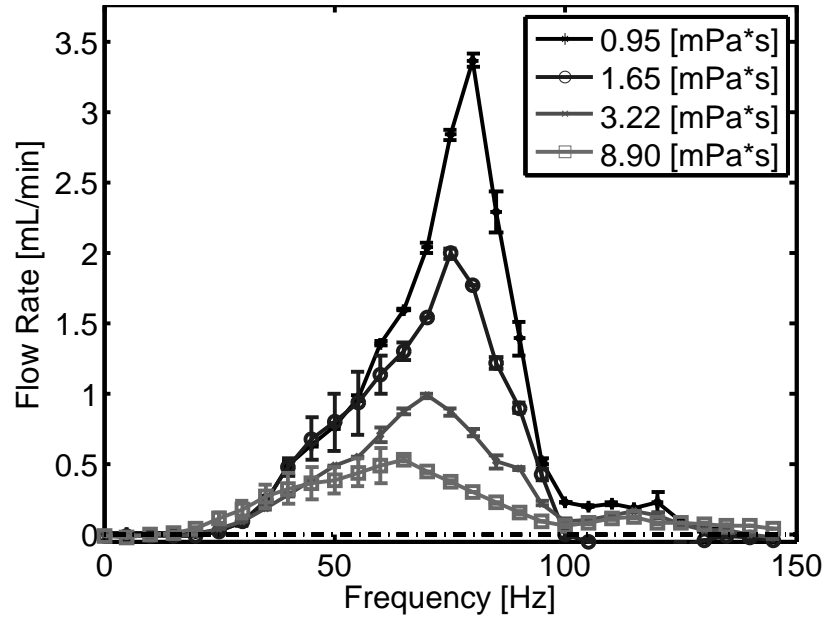


Figure 3.21: Planar White-Stiff membrane (1.4 MPa) performance as a function of fluid viscosity ( $x = 5$  mm,  $y = .5$  mm,  $A = 0.4$  mm, valves = closed)

## Bibliography

- A. I. Hickerson. *An Experimental Analysis of the Characteristic Behaviors of an Impedance Pump*. PhD thesis, Caltech, 2005.
- S. Takagi and K. Takahashi. Study of a piston pump without valves .2. pumping effect and resonance in a pipe-capacity-system with a t-junction. *Bulletin of the Japan Society of Mechanical Engineers*, 28(239):831–836, 1985.
- M. Zamir. *The Physics of Pulsatile Flow*. Biological Physics Series. Springer-Verlag New York, New York, 2000.

## Chapter 4

# Discussion and Analysis

### 4.1 Reynolds Number and Womersley Number Scaling

To get a better sense of the dynamics of the pump and flow loop, it is useful to investigate the Reynolds number, Equation 4.1. The Reynolds number will give us insight into how important the fluid inertia of the system is in determining the flow behavior.

$$Re_d = \frac{\rho U d}{\mu} = \frac{4\rho Q}{\pi\mu d} \quad (4.1)$$

Since we have looked at both planar pumps and tubular pumps in the same flow loop, it is helpful to analyze both the loop and the pumping elements separately. The flow loop was approximately 75 cm long and consisted primarily of 1.5 mm I.D. rigid plastic tubing with an 8.5 mm long section of 2 mm I.D. plastic tubing where the flow meter was placed. There are four flow contractions on either side of the prime-purge valves where the rigid plastic tubing connects. A syringe pump was used to impart a steady flow through the loop and the pressure drop was measured. A flow rate of 6 mL/min caused a pressure drop of 1 kPa across the loop, values consistent with average flow and pressure data taken during valveless pump tests. Assuming fully developed Hagen-Poiseuille flow, Equation 4.2 can be used to calculate an effective loop diameter of 1.32 mm, consistent with the physical construction of the loop. Table 4.1 summarizes the Reynolds number for the maximum achieved net flow rate for each pumping element and the flow loop. Instantaneous flow rates two or three times greater than these maximum net flow rates were seen in the oscillatory component of the signal.

$$\Delta P = \frac{8\mu L Q}{\pi r^4} \quad (4.2)$$

Pump	Max Q [mL/min]	Effective $d_{pump}$ [m]	Effective $d_{loop}$ [m]	$Re_{d_{pump}}$	$Re_{d_{loop}}$
Thin	2.9	0.0018	0.00132	34	47
Thick	8.2	0.0015	0.00132	116	132
Planar	3.5	0.0032	0.00132	23	56

Table 4.1: Summary of characteristic Reynolds numbers for the pumping elements and the flow loop with water as a working fluid

Womersley number, Equation 4.3, gives us similar information to the Reynolds number about the inertial versus viscous forces, but for the oscillatory component of the flow. For an excitation frequency of 140 Hz, the characteristic diameter of the flow loop calculated above ( $d_{loop} = 1.32mm$ ), and water as a working fluid, the calculated Womersley number is  $\alpha = 20$ . Womersley number greater than  $\alpha = 10$  is considered moderately high, and the values seen in this experiment indicate a relatively flat, plug-like velocity profile with the flow lagging the pressure by a phase shift of about 90 degrees. Coincidentally, these Womersley numbers match well with the values of Hickerson (2005). Hickerson’s experiments corresponded to Womersley numbers up to approximately 30.

$$\alpha = \sqrt{\frac{\pi}{2} ReSt} = r \sqrt{\frac{2\pi f \rho}{\mu}} \quad (4.3)$$

It should be noted that for Womersley number greater than 10 in a completely rigid tube, the amplitude of the oscillatory flow response to the oscillatory pressure gradient will be less than 10% that of a DC flow response to a DC pressure gradient of the same amplitude. As the Womersley number increases, the oscillatory flow response tends to zero, assuming a completely rigid tube. Therefore, any significant oscillatory flow component seen in these high Womersley number cases is due to compliance in the system. This knowledge can be used to tune the oscillatory component of the flow for applications that might require the increased mixing or heat transfer that comes from larger flow oscillations. Zamir (2000) provides an excellent overview of Womersley number analysis for pulsatile flow in rigid and elastic tubes.

## 4.2 Transient Behaviors at Startup and Relaxation

### 4.2.1 Startup

One of the unique features of the study described in this thesis is the ability to analyze high resolution dynamic data at the startup and relaxation of a pump excitation to gain insight into the mechanisms responsible for driving net flows. Figure 4.1 shows some typical transient pressure and flow data for a thin-walled tube excited at 65 Hz. The measured position of the excitation probe was also plotted to give the reader a sense for how quickly the pressure and flow respond to the

excitation. The flow regime seen for this case is very steady with a high mean value of almost 3 mL/min and a very small oscillatory component. This flow regime can be contrasted to that seen in Figure 4.2 of transient flow in an excited thick-walled pump that has a very large oscillatory component relative to the mean flow value. These two flow regimes represent two extremes of flow behaviors seen in valveless pumps: high DC flow content with low AC content and high DC flow content with high AC content. The other two combinations, low DC/high AC and low DC/low AC were also observed in the experiments carried out for this study.

For the thin-walled case under investigation, the flow rate takes approximately 15 excitation cycles to reach its steady-state value. However, this long build up time is likely a result of the low characteristic Reynolds number of the system described in Section 4.1 rather than being caused by some build up of pump dynamics. In fact, if the reader looks at the transient differential pressure in Figure 4.1, it can be seen that the steady-state differential pressure is achieved almost immediately, within two cycles. The differential pressure even appears to overshoot, because the fluid in the system is slow in acceleration to its steady-state value.

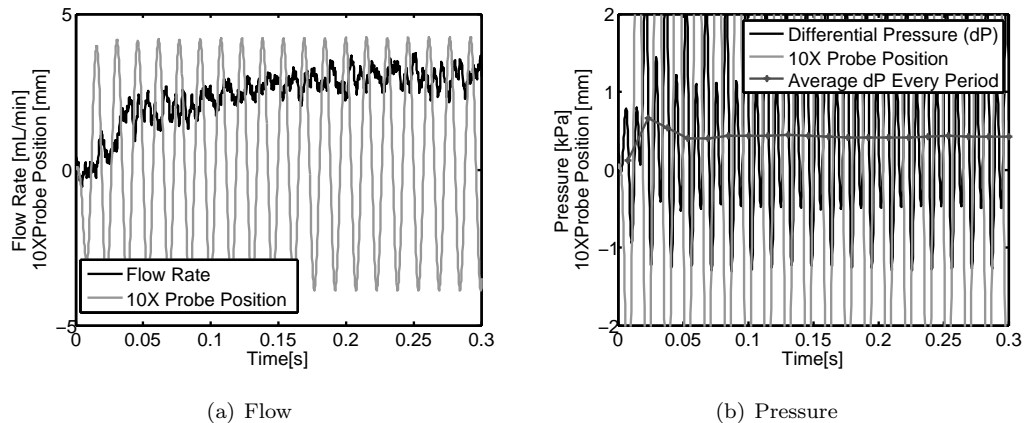


Figure 4.1: The startup of the Latex Thin tube excited at 65 Hz ( $x = 5$  mm,  $y = 1.2$  mm,  $A = 0.4$  mm, vents = closed)

Figure 4.2 shows very different behaviors for the thick-walled excitation transients when compared to the thin-walled excitation transients. One thing to note is that the mean steady-state flow rate in the thick-walled case is actually twice as high as that in the previously discussed thin-walled case. While the mean value is relatively high, approximately 6 mL/min, it is shrouded in a large oscillatory flow component that actually goes negative every cycle. One potential reason for the large oscillatory component in this case could be the fact that the right side of the tube has been vented to atmospheric pressure. Other than the venting, the thin-walled and thick-walled tubes discussed in this section have very similar excitation parameters but, as the reader can see, they

have very different pressure and flow responses due to differences in tube material properties and venting.

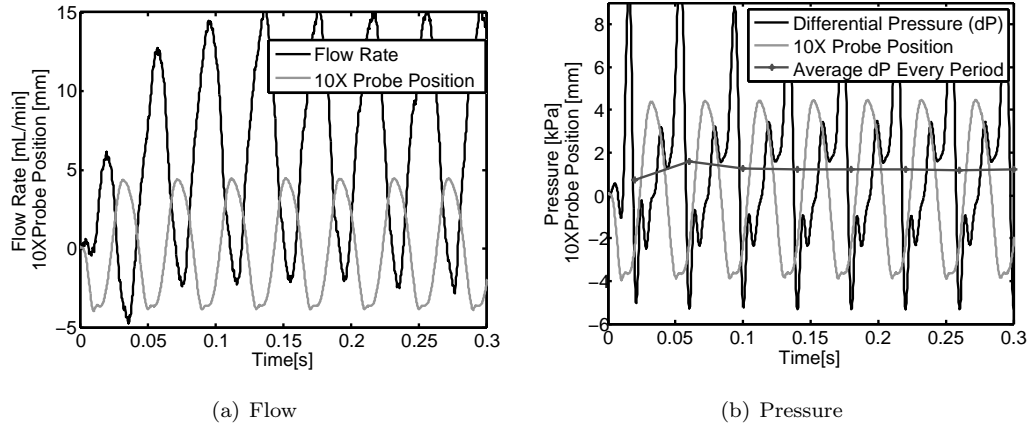


Figure 4.2: The startup of the DOW006-2cm tube excited at 25 Hz ( $x = 5$  mm,  $y = 1.1$  mm,  $A = 0.4$  mm, vents = right open)

#### 4.2.2 Relaxation

Figure 4.3 is the relaxation event after the pump described in Figure 4.1 has been excited for 3 seconds. The relaxation transients tell a similar story to the startup transients. The flow rate is slow to come to rest, but the pressure responds almost immediately.

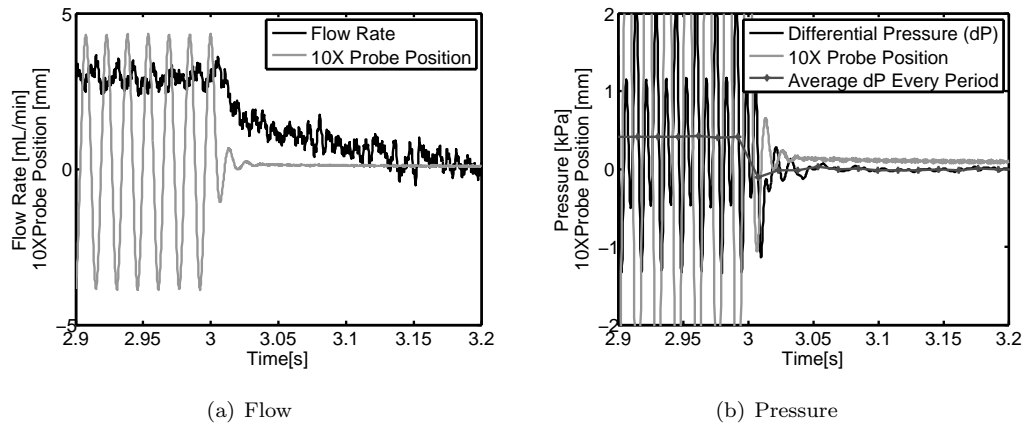


Figure 4.3: The relaxation of the Latex Thin tube after being excited at 65 Hz ( $x = 5$  mm,  $y = 1.2$  mm,  $A = 0.4$  mm, vents = closed)

Figure 4.4 is the relaxation event after the pump described in Figure 4.2 has been excited for 3 seconds. One interesting feature seen here is that the flow rate continues in a damped oscillation to rest for a few cycles after the excitation has stopped. This is most likely a consequence of the

venting of the right side of the tube, which leads to a flow loop of effectively infinite compliance.

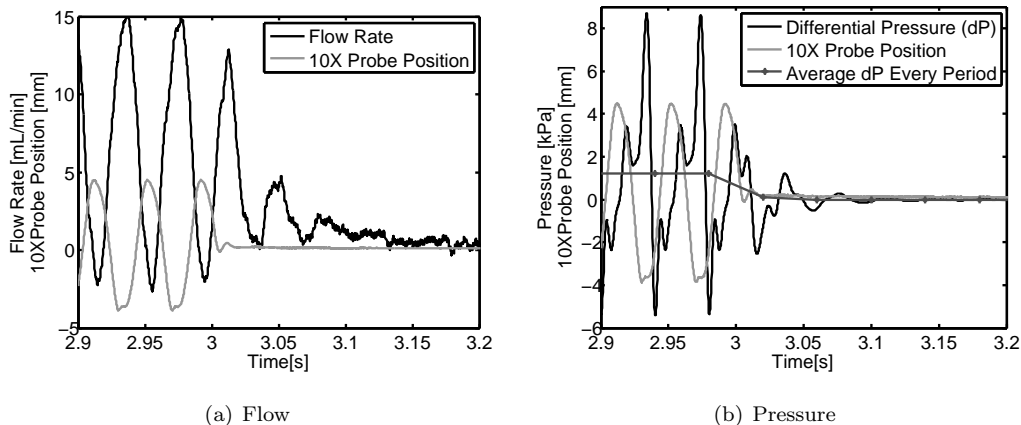


Figure 4.4: The relaxation of the DOW006-2cm tube after being excited at 25 Hz ( $x = 5$  mm,  $y = 1.1$  mm,  $A = 0.4$  mm, vents = right open)

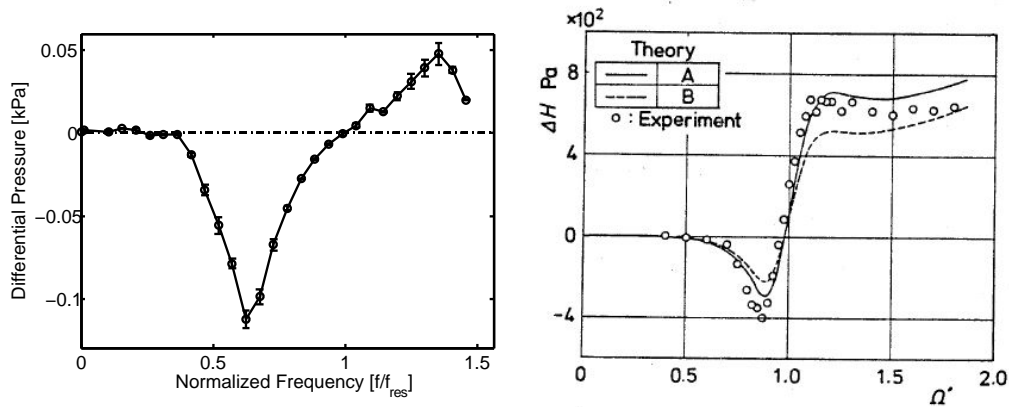
### 4.3 Comparison to Previous Studies

The only extensive experimental study available to compare with is that of Hickerson (2005) on a 2 cm diameter pump. Many qualitative behaviors were preserved, even though the length scales of the present study are an order of magnitude smaller. All tubes and membranes in the current study showed apparent resonant behavior, frequency-dependent flow reversals, and sensitivity to excitation amplitude and offset. The behaviors of the thin-walled tube and the planar pumps matched most closely with the experiments of Hickerson (2005). One prominent feature of valveless pumping based on the Liebau phenomenon, which has been mentioned in almost every study of valveless pumping, is the symmetry of flow performance with respect to the middle of the length of the pumping element. This feature was preserved in the thin-walled and planar studies, but was not seen in every case of the thick-walled tube.

While every pumping element showed apparent resonant behavior, the limited bandwidth of excitation and measurement capabilities means that only the thin-walled and planar pumps were excited at the critical resonant frequency defined by Hickerson (2005) (the wave speed in the pump divided by two times the pump's length). For these two systems, Hickerson's critical resonant frequency did appear to predict a resonant peak, but significant resonance occurred at frequencies below this value as well.

An interesting comparison in resonant behavior is seen between the thin-walled pumps in this

study and the experiments and modeling of Takagi and Takahashi (1985) and Borzi and Propst (2003). Takagi and Takahashi (1985) measured the damped natural frequency of their asymmetric T-junction pump through a small perturbation. They then discovered an interesting flow behavior when the system was excited around this natural frequency, namely that large net flow was generated on either side of the natural frequency with opposite sign and no net flow was generated at the natural frequency. Borzi and Propst (2003) observed the same behavior in their numerical model of the Liebau phenomenon. It was earlier shown that when the thin-walled pumps in this study were perturbed, they resonated at 96 Hz. Figure 4.5 shows data from the thin-walled pump in this study with its excitation frequency normalized by this damped natural frequency. The similarity in behavior to Takagi’s T-junction pump and Borzi’s numerical results is striking. It should be noted that the frequency of free oscillation of the thin-walled pump, or any other pump or membrane in this study, does not match the critical resonant frequency predicated by Hickerson.



(a) Normalized differential pressure data from thin-walled pump

(b) Data from Takagi and Takahashi (1985)

Figure 4.5: Note that the definition of differential pressure for this study has been inverted to match that of Takagi

The wave speed in the thick-walled tube placed Hickerson’s critical resonant frequency far out of reach of this experimental setup. The thick-walled tube still displayed apparent resonant behaviors, but in other ways deviated greatly from the expected valveless pump behavior. Most surprisingly, the thick-walled pump performance did not show symmetry with respect to length of the pumping element. Such a behavior has never been described in the valveless pumping and Liebau phenomenon literature.

Based on the extensive loop and pumping element characterization performed for this study, the conclusion reached is that the thick-walled tube’s behavior is caused by similarity in compliance to the flow loop. While the thick-walled pump is more compliant than the loop, they are on the same

order of magnitude and differ by approximately a factor of 5. The 2 cm long thick-walled AB tube has a compliance of between 3-8 1/MPa, while the flow loop has a measured compliance of 0.7-1.2 1/MPa. Compare these values to the approximately two orders of magnitude lower compliance for the thin-walled tubes (45-74 1/MPa) and planar pumps (90-339 1/MPa). When the compliance of the pump and the flow loop are so similar, the flow loop effectively becomes part of the pump. Therefore, changing excitation location across the thick-walled membrane has little effect on the effective excitation location of the larger system. While great care was taken to ensure a symmetric experimental flow loop, clearly small asymmetries still exist that allow valveless pumping to occur in this scenario. Particularly, impedance mismatches occur at any point where a diameter change or curvature change in the tube wall takes place.

Further support for this conclusion comes from the variation of inlet/outlet pressure conditions on the thick-walled tube. When the loop is vented to atmospheric pressure on both sides of the pump, effectively driving the loop compliance to infinity, the symmetry with respect to length on the tube returns (Figure 3.11). Also, when only one side of the pump or the other is opened to atmosphere, the frequency response is inverted, because the effective compliance of each side is inverted (Figure 3.13 and Figure 3.14). This result has important implications for small scale devices that may be fabricated using multilayer soft lithography or other techniques that could lead to a pumping element and flow loop of comparable compliance.

## 4.4 Pump Curve

One of the goals of this study was to create a pump curve for a valveless pump to investigate its behavior across a range of loop resistance. The data for the thin-walled pump loop-resistance study can be seen in Figure 3.8, and Figure 4.6 below summarizes the differential pressure, flow, and mean flow power at five different operating conditions for an excitation frequency of 60 Hz. The pump curve shows features consistent with traditional macroscale pumps, such as an increasing pressure head for increased flow resistance.

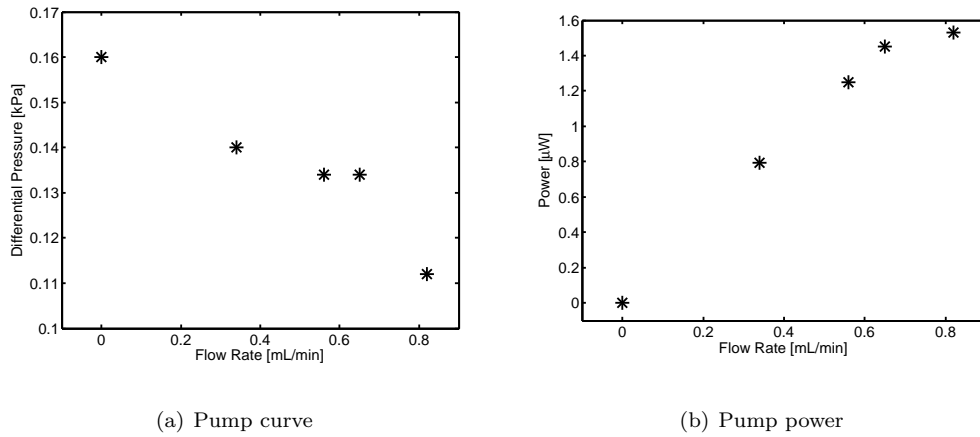


Figure 4.6: Pump curve for thin-walled elastic tube under five different operating conditions (distinct loop resistances)

## 4.5 Viscosity and Density

When the viscosity of the working fluid was increased in the thin-walled tube, the net flow rate in the system decreased. This is expected, because the fluid resistance of the loop will increase with increasing viscosity, and in the case of Hagen-Poiseuille flow, the resistance would scale linearly with viscosity (Equation 4.2). The unexpected result comes from the fact that the differential pressure generated by the pump increases dramatically as the viscosity and, more importantly, the density of the working fluid increases. One way to decouple the density effects from the viscous effects is to look at the pump curve in Section 4.4. From the pump curve, we know to expect a differential pressure increase on the order of 50% from the original loop configuration to infinite resistance. However, as the reader can see in Figure 3.9, the differential pressure generated by the pump doubles for a working fluid density of only 19%. The fluid viscosity across the study varied approximately by a factor of 30, but in every case the thin-walled tube was able to pump the fluid. The added

resistance from the increased fluid viscosity was partially countered by the accompanying increase in fluid density. Density of the working fluid is clearly a critical factor in determining the ultimate performance and efficiency of the valveless pumping phenomenon. This effect was also observed in the planar pumps, but not in the thick-walled tube. It is hypothesized that relative magnitudes of elastic forces to inertial forces are playing a key role in whether or not this behavior is observed.

## 4.6 Efficiency

### 4.6.1 Volumetric Efficiency

The volumetric efficiency of valveless pumps based on the Liebau phenomenon is often claimed as a benefit over other types of pumping. The practice of nondimensionalizing the flow rate by the rate of fluid displacement of the excitation is carried out in numerous theoretical analyses. Motivated by this practice, Hickerson (2005) also looked at the nondimensional flow rate of the pump defined in this manner. The difficulty however, comes in defining exactly how much fluid is displaced by one cycle of excitation. Unlike 2D and 1D models, the physical pump deforms in three dimensions. The cross section of the pump becomes an oval as it is compressed, rather than the actuator sweeping a simple volume. It is not clear how Hickerson (2005) accounted for this in her calculations of nondimensional flow rate. In the present study, the fluid displaced as a function of probe depth was physically measured by attaching a capillary of known inner diameter to one of the prime/purge valves while the rest of the system is closed. The fluid displaced by the probe motion and the tube deformation is recorded as a fluid height change in the capillary. For an excitation displacement of 0.8 mm, the displaced fluid volume was found to be  $1.78 \mu\text{L}$  for the thin-walled tube,  $2.22 \mu\text{L}$  for the thick Allied Biomedical tube, and  $2.88 \mu\text{L}$  for the thick Dow Silastic-006 tube. These values were used to nondimensionalize the results in Figure 4.7.

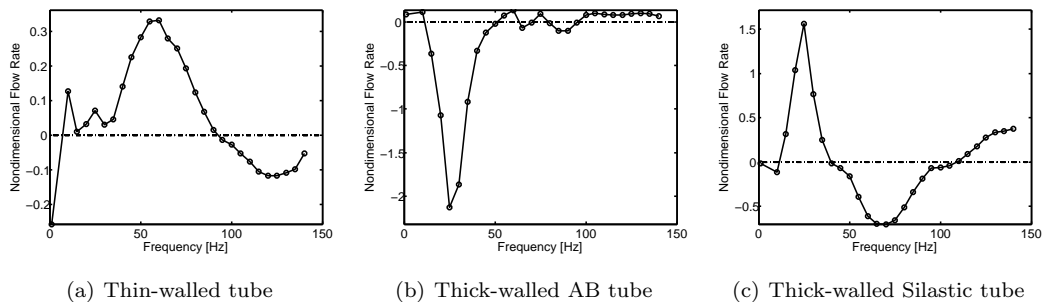


Figure 4.7: All three pump tests shown above were performed with the following parameters:  $x = 5$  mm,  $y = 1.1$  mm, and  $A = 0.4$  mm (0.8 mm total displacement). The right vent was open for the two thick-walled cases, and the loop was closed for the thin-walled case.

Figure 4.7 shows some very intriguing behavior. Volumetric efficiencies around 0.5 are common at resonance in many valveless pump references, however achieving a nondimensional flow rate greater than unity has never been reported for this definition of normalization. Continuity prevents a true volumetric efficiency greater than unity, and even approaching unity at these Reynolds numbers would be very unlikely. The most likely explanation is related to the open vent coupling with the tube dynamics to greatly increase the volume displaced in the pumping element in each cycle. It is clear from the data that this 30 Hz resonance is related to opening the flow loop to atmospheric pressure on one side or the other for thick-walled tests.

#### 4.6.2 Pump Power and Efficiency

Calculating a true mechanical efficiency of this valveless pumping mechanism would be very valuable for designing self contained lab-on-chip and medical devices. There was an effort to measure the dynamic force exerted on the membrane using an Omega linear force transducer in line with the probe. It turned out that the acceleration forces due to unsprung mass below the force transducer, made resolving the actual component related to exciting the membrane very difficult. However, the linear force transducer was used to capture the force to both deflect the membrane at a constant displacement and at very low frequencies. In the planar pump configuration, the stiffest membrane (1.4 MPa) required approximately 0.25 N/mm for deflections less than 1 mm. This value can be assumed as the amplitude of the oscillatory excitation force to get an order of magnitude estimate for the mechanical efficiency of the planar pump configuration.

In Figure 3.20, the reader can see a case where the stiffest planar pump membrane achieved a net flow rate of 3.5 mL/min at a resonance excitation frequency of 80 Hz. The corresponding differential pressure for this case was 0.507 kPa, making the steady-state flow power approximately 29.58  $\mu$ W. Next, we can estimate the input power, assuming a sinusoidal displacement of the membrane at 80 Hz with amplitude 0.4 mm and a sinusoidal force profile with amplitude 0.1 N. Using Equation 4.4, and considering that work is only done on the downstroke of the excitation, we get that work is being done on the membrane at a rate of 3.2 mW. If we then define the mechanical efficiency of the pump as the flow power divided by the rate of work being performed on the membrane, we get an efficiency of approximately 1% at this resonant flow condition. The true force to dynamically excite the membrane is undoubtedly higher than this estimate from static force measurements, so it appears that while the Liebau phenomenon may be very efficient from a volumetric perspective, mechanical efficiency is not one of its benefits.

$$P_{ave} = \frac{1}{T} \int_0^T \vec{F} \cdot \vec{v} dt \quad (4.4)$$

In order to compare the expected efficiency of an impedance pump based device with that of a commercially available micropump, it is also necessary to estimate the mechanical efficiency of a potential actuation scheme. For a planar impedance pump, a piezoelectric bending actuator could provide the necessary force, displacement, and frequency of excitation necessary to drive flows described in this thesis. The efficiency (output mechanical energy/input electrical energy) of a unimorph piezoelectric bending actuator is on the order of 2% (Wang et al., 1999), placing the overall mechanical efficiency estimate of a planar impedance pump actuated with a piezoelectric bending actuator at approximately 0.02%. While this number appears prohibitively low, it should be noted that a commercially available MDP1304 micro diaphragm pump from thinXXS Microtechnology ([www.thinxxs.com](http://www.thinxxs.com)) has an overall mechanical efficiency of 0.3% for a 2 mL/min flow rate at 20 kPa backpressure. Mechanical efficiency is likely not a critical characteristic of microscale pumps, because even accounting for the use of a very inefficient actuation scheme like the unimorph piezoelectric, this manifestation of an impedance pump could dispense over 10,000 fluid samples of 100  $\mu\text{L}$  in a medical or LOC application using the energy in one Duracell 2430 Lithium Battery, approximately the size of a quarter.

#### 4.6.2.1 Inefficiency Leading to Heating of the Working Fluid

The total fluid volume of the flow loop in this study was 1.3 mL. In the efficiency calculations, work is being done on the membrane at an estimated rate of 3.2 mW for a resonant flow case (80 Hz and 0.4 mm amplitude). Assuming all of this energy gets dissipated into heat in the working fluid, the water in the flow loop would increase in temperature by 1  $^{\circ}\text{C}$  every 30 minutes of continuous operation. In the studies presented in this thesis, the pump was never run for more than 15 seconds continuously. The power put into the membrane increases with the square of the frequency and linearly with the amplitude of the force of excitation and amplitude of the displacement of excitation. The force and displacement can be related with knowledge of the membrane elastic modulus and the specific geometry of the pumping element. Heating of the working fluid could become a concern for long operation times at the size scales studied in this thesis as well as at smaller size scales.

## 4.7 Offset and Amplitude

The excitation amplitude and offset was easily adjusted in the present study. Many previous references suggest that there is a linear dependence on excitation amplitude and offset, however the data shown in Figure 4.8 appears to be sinusoidal in nature. A sinusoidal dependence on excitation amplitude and offset matches intuition for compressing the circular cross section of a tube. As you sweep down through an undisturbed tube, each unit moved down sweeps an incrementally larger volume until the midpoint of the tube is reached. Once compressing past the midpoint of the tube,

each unit moved down sweeps an incrementally smaller volume until you reach the opposite side of the tube. A linear dependence on excitation amplitude and offset would only be valid for an ideal 1D or 2D compression in a model or simulation.

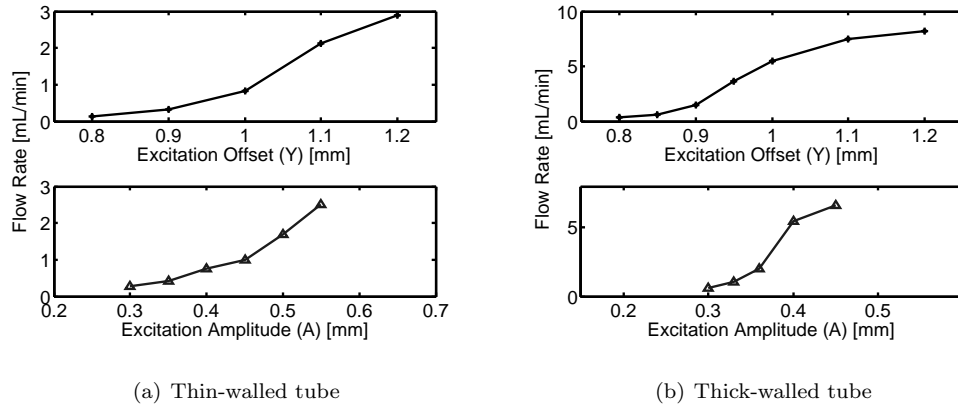


Figure 4.8: The effect of excitation amplitude and offset on net flow rate for a thin-walled tube excited at 60 Hz and a thick-walled tube excited at 30 Hz. During offset variation, the amplitude was held fixed at 0.4 mm and during amplitude variation, the offset was held fixed at 1.0 mm.

## 4.8 Transmural Pressure

Hickerson (2005) investigated the effect of transmural pressure on pump performance, and found that as transmural pressure increased, so did the frequency at which peak flow occurred. This increase in frequency is consistent with an increase in tube wall tension, leading to higher wave speeds and resonant frequencies. Again, we see agreement with behaviors observed by Hickerson (2005) for the thin-walled tubes, but not for the thick-walled tubes. Figure 3.7 shows an increase in resonant flow peaks to higher frequencies for increased transmural pressure in thin-walled tubes. However, Figure 3.15 shows that a similar increase in transmural pressure in the thick-walled tube has essentially no effect on the flow performance or resonant flow peaks of the pump. This could be explained by the lower compliance in the thick-walled case making the increase in transmural pressure insignificant at these pressures, or it could indicate that there is a fundamentally different flow and pressure generation mechanism at play for the thick-walled tubes. To test transmural pressures high enough to impart significant wall strain in the thick-walled tubes would require pressures above the rating of the pressure transducers used in this study and other transducers with the correct form factor for the characterization system were not readily available.

## Bibliography

- A. Borzi and G. Propst. Numerical investigation of the Liebau phenomenon. *Zeitschrift Fur Angewandte Mathematik Und Physik*, 54(6):1050–1072, 2003.
- A. I. Hickerson. *An Experimental Analysis of the Characteristic Behaviors of an Impedance Pump*. PhD thesis, Caltech, 2005.
- S. Takagi and K. Takahashi. Study of a piston pump without valves .2. pumping effect and resonance in a pipe-capacity-system with a t-junction. *Bulletin of the Japan Society of Mechanical Engineers*, 28(239):831–836, 1985.
- Q.-M. Wang, X.-H. Du, B. Xu, and L. E. Cross. Electromechanical coupling and output efficiency of piezoelectric bending actuators. *IEEE Transactions on Ultrasonics, Ferroelectrics and Frequency Control*, 46(3):638–646, 1999.
- M. Zamir. *The Physics of Pulsatile Flow*. Biological Physics Series. Springer-Verlag New York, New York, 2000.

## Chapter 5

# Conclusion

### 5.1 Summary of Important Findings

In addition to the discussion and analysis provided in the previous chapter, it is useful to go back and revisit the major questions from the introduction of this thesis.

- Which behaviors previously observed on large scale impedance pumps scale down to microscale valveless pumps?

Every experimental observation made for the 2 cm diameter pumps in Hickerson (2005) was repeated in this study for pumps an order of magnitude smaller. It appears that all of the known behaviors of valveless pumps based on the Liebau phenomenon scale down at least to the size scales investigated here, with characteristic diameters on the order of 1 mm.

- Which parameters from Table 1.1 are most important in determining the performance of a valveless pump?

Spatial parameters of the excitation appear to have a strong, but clear, influence on the performance of valveless pumps. For a given excitation frequency the generated flow scales linearly with the volume of fluid displaced. However, for different pump geometries the volume of fluid displaced does not necessarily scale linearly with excitation amplitude or offset. Temporal parameters of the excitation, such as excitation frequency, have a drastic, nonlinear effect on pump performance.

Compliance, a combination of elastic modulus, wall thickness, and pump length scales, has also been shown to be a critical parameter in determining fundamental pump behavior. The effects of compliance will be discussed in more detail below.

The working fluid viscosity was shown to be an important factor as it relates to flow resistance,

however the valveless pumps studied here showed robust performance in their ability to pump fluids with viscosity an order of magnitude greater than water. The working fluid density was shown to be much more fundamental in changing pump performance, likely due to the increased mass affecting the resonant phenomenon responsible for increased flow generation at resonant peaks.

Transmural pressure was shown to affect the frequency of resonant peaks, but only if the magnitude of the pressure is significant relative to the compliance of the system.

- What level of prediction of pump direction at different frequencies can be achieved?

A general statement about flow direction can be made from analyzing all of the data sets presented. If the excitation location is used as the point of reference, the first resonant flow peak always occurred with flow in the direction of least compliance. An intuitive explanation for this observation is that at lower frequencies the local pressure increase created by the compression of the excitation is higher in the less compliant section (shorter length of pump or unvented side) and lower in the more compliant section (longer length of pump or vented side). The resulting pressure differential drives flow around the flow loop. At the frequency that the pumping element freely resonates, the excitation location is less important and the pump produces little or no flow due to a symmetric oscillation along its entire length. At frequencies above the freely resonating frequency of the pumping element, the dynamics reverse and a pressure differential is generated in the opposite direction.

- What effect will increased fluid density and viscosity have on microscale valveless pump performance?

This study has shown small scale valveless pumps capable of pumping highly viscous fluids. It was also discovered that the density of the working fluid plays an important role in the energy transfer from the excitation to the pumping. No fundamental difference was observed in the pump operation with viscous working fluids, other than a slight resonant frequency shift that is likely related to the change in density of the fluid. It is expected that this resonant frequency shift scales as  $\frac{1}{\sqrt{\rho_{fluid}}}$ , but this frequency shift for the range of fluid densities explored in this study is on the order of 5 Hz, the resolution of the frequency sweeps performed to investigate the frequency dependent flow behavior. However, frequency shifts are qualitatively evident.

- How do the dynamics of planar valveless pumps differ from tube-based pumps?

This study verified that planar pumps showed the same performance behaviors as one would expect from a tube-based pump of similar size scale. This is a promising result, because planar pumps are much more practical for many potential applications and manufacturing techniques.

- What are the most important parameters to consider when designing a microscale system or device utilizing a valveless pump?

This study has identified the relative compliance of the pump to the system it is working on as a critical factor in the behavior and performance of valveless pumps. It appears that a pump of substantially different compliance, either much larger, or much smaller than the loop or system it is working on can be designed and characterized outside of the system and then expected to behave in a known manner once implemented. However, if the compliance of the loop or system is on the order of the compliance of the pump, the two become coupled and the pumping dynamics and performance cannot be separately determined. This result has important implications for small scale devices that may be fabricated using multilayer soft lithography or other techniques that could lead to a pumping element and flow loop of comparable compliance.

- Can a valveless pump be treated as a stand-alone device, or is its fundamental behavior always a function of the system it operates on?

The consideration of the relative volumetric compliance of the pump to the system it operates on is critical in determining whether the pump can be characterized independently.

- What can be said about the efficiency of valveless pumps beyond the volumetric efficiency approach of previous literature?

The small scale pumps investigated in this study showed similar and in some cases higher volumetric efficiencies than the already high values quoted in previous literature for larger pumps. An estimate of the mechanical efficiency of this valveless pumping phenomenon shows that on the order of 1% of the work put into deflecting the membrane makes it into the fluid as useful flow work.

- What different flow regimes exist as outputs of valveless pumps? Can a periodically excited valveless pump put out a steady flow rate?

Surprisingly steady flow rates were observed for the thin-walled pumps studied here. Any combination of high and low net flow and high and low oscillatory component can exist as the output of the valveless pumps described here. The Womersley number of the flow loop can be used to estimate the relative magnitude of the oscillatory component of the flow. For Womersley number greater than 10, i.e. high frequency actuation, the amplitude of the oscillatory flow is very low compared to the amplitude of oscillatory pressure gradient. However, it should be remembered that this only applies to rigid, closed systems, and if significant compliance is added at some point in the system, volume changes in that region can lead to significant oscillatory flow.

- What are the transient behaviors of small scale valveless pumps, and what are the implications for practical devices?

The transient behavior of valveless pumps on this size scale showed to be surprising abrupt. The steady-state differential pressure was achieved almost immediately, within the first two excitation cycles. In some cases, the flow rate appeared to follow the generated pressure head and reach a steady-state value after a slow acceleration, but in other cases the steady-state flow rate was achieved as the mean of a highly oscillatory flow apparently driven by the excitation within the first few excitation cycles.

## 5.2 Future Directions

### 5.2.1 Computational Modeling

The characterization system designed and built for this study has produced much more data than could possibly be processed and analyzed for this thesis. The high resolution dynamic data could be extremely useful for validation of computational models that would make the study of the vast parameter space described in Table 1.1 more realistic.

### 5.2.2 Membrane Tracking using DDPIV

As the study of the Liebau phenomenon shifts to planar pumps for practical devices, the three-dimensional dynamics of the pump membranes are an interesting area for new research. We considered investigating the planar membrane dynamics experimentally using the micro DDPIV technique. Ultimately, this part of the study was not carried out, but some interesting results were achieved related to the sensitivity equations for multiple lense and microscope-based DDPIV systems and are shown in Appendix C. The study of planar valveless pump membrane dynamics is an interesting and important area for future research.

### 5.2.3 Attached Actuators

One limitation of the study presented here is that the excitation probe was not attached to the pump wall. In almost any practical device, an excitation scheme would be firmly attached to the pump and provide an expansion force as well as a compression force. Investigation of how this change in actuation implementation affects pump performance and dynamics would be extremely valuable.

## **5.2.4 Other Valveless Pumping Scenarios of Interest**

### **5.2.4.1 Ocean Wave Energy Capture**

Many other scenarios exist where valveless pumping could be extremely beneficial. The data and analysis in the current thesis has shown that the Liebau phenomenon scales down well across multiple orders of magnitude. It would be interesting to study how large of a system could achieve similar valveless pumping behaviors. In particular, a preliminary study was executed showing that the Liebau phenomenon can be extended to systems with a free surface. The results of this preliminary study are summarized in Appendix D. If valveless pumping could be scaled up to the length scales present in free surface ocean waves, the Liebau phenomenon could be an extremely promising form of renewable energy generation through ocean wave energy capture.

### **5.2.4.2 Impedance Pump with Valves**

In some applications it may be beneficial or necessary to place valves or other flow regulation inline with a valveless pump. A preliminary study was carried out to investigate what effect valves might have on the pumping behavior of valveless pumps, effectively turning them into positive displacement pumps. The data of this short study can be found in Appendix E. Further study of systems like this and more generally valveless pumps incorporated with other components of potential lab-on-chip devices will be a critical step in the utilization of valveless pumps in real engineering systems.

## Bibliography

- A. I. Hickerson. *An Experimental Analysis of the Characteristic Behaviors of an Impedance Pump*.  
PhD thesis, Caltech, 2005.

## Appendix A

# Data Acquisition System Verification

Great care was taken to ensure reliable, unbiased data with known accuracy and confidence limits.

The NI PCI-6035E has a capacity of 16 single ended or 8 differential analog input channels. For the majority of my experiments, 4 differential analog input channels were used (LVDT, Flow, Pressure Transducer 1, and Pressure Transducer 2), as well as 1 analog output to the amplifier driving the BK Voicecoil. The NI PCI-6035E is capable of 200 kS/s across all inputs, which then limits the available sample rate of individual inputs. For example, if the sample rate is spread evenly across four inputs, each channel can sample at 50 kS/s.

One unique aspect of this study was the ability to get high resolution dynamic information related to the pressure and flow output of the impedance pump. However, because our DAQ was not capable of simultaneous sampling between channels, it was necessary to characterize the time lag between input channels in order to perform a reliable time-based comparison of dynamic information from the input channels.

The accuracy of the measurement on the analog input channels is proportional to the range set when the input channel is initialized and is approximately .05

To test the limits of the DAQ, a function generator was used to supply 0.1 V (1000 Hz and 5000 Hz). The time lag between channels 1 and 4 appeared to be at most, one time step at a 50,000 Hz sampling rate or 20 microseconds.

The charging time of the multiplexer was also a concern since this is not a simultaneous sampling DAQ system. In the end the KH Model 3988 was utilized to lower the output impedance of the pressure transducers. Completely independent loads were applied to all four measurement devices (two pressures, one LVDT displacement, and one flow rate) in the system to check the ability of the DAQ to measure all of the channels independently without the problem of ghosting in any channels.

The ability of the DAQ to measure between a large voltage swing was also tested. Ghosting occurs when the impedance of the source is too high to come to equilibrium with the voltage on the

multiplexer in the sampling time.

The highest voltage was seen on the input from the flow meter, so to test the system's ability to react to such large voltage swings, a function generator was set to a 200 Hz sine wave with an amplitude of 3 V (6 V peak-to-peak). Figure A.1 shows the results of one of the verification tests, to make sure the multiplexer in the DAQ has sufficient time to accurately sample data from each channel without ghosting effects.

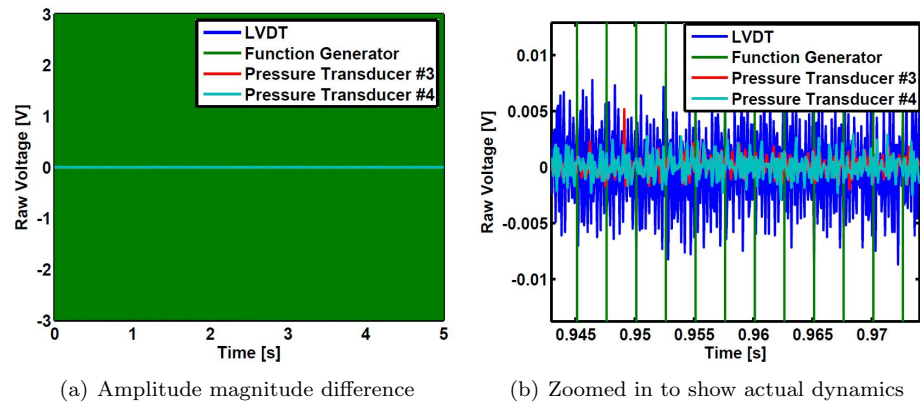


Figure A.1: Verification of DAQ Settings. The imposed high voltage signal does not bleed into the other data acquisition channels.

## Appendix B

# Viscosity Sample Verification

A Gilmont Instruments GV-2200 Size #2 falling ball viscometer was used to measure the viscosity of each of the working fluids used in the scaling studies of the impedance pump. The viscometer was initially calibrated using Cannon Instrument Company viscosity standards N1.0 and S3. Water and glycerine solutions were used, because of their compatibility with the pumping and loop materials as well as the ability to test a wide range of viscosity with relatively small change in density. Table B.1 shows the results of the viscosity sample preparation and calibration.

Sample	Mass H <sub>2</sub> O [g]	Mass Glycerine [g]	Glycerine Content [%]	Published Viscosity [mPa*s] @20°C	Published Density [kg/m <sup>3</sup> ] @20°C	Measured Viscosity [mPa*s] @23°C	Measured Density [kg/m <sup>3</sup> ] @23°C
H <sub>2</sub> O	100	0	0	1.005	0.998	0.95	1.00
20%	70.04	20.01	20.0	1.76	1.04690	1.65	1.05
40%	62.54	41.68	40.0	3.72	1.0993	3.22	1.10
60%	40.06	60.1	60.0	10.8	1.1538	8.90	1.15
70%	30.06	70.14	70.0	22.5	1.1813	18.16	1.18
75%	25.05	75.15	75.0	35.5	1.1949	28.23	1.19
80%	20.03	80.07	80.0	60.1	1.2085	45.71	1.20

Table B.1: Results of viscosity measurements

One important thing to note about water and glycerine solutions is the sensitivity of their viscosities to temperature change. The viscosity of water is notoriously sensitive to temperature, and glycerine is even more sensitive. This temperature sensitivity accounts for some the discrepancy seen between the published viscosity values at 20°C and the measured values at 23°C. Figure B.1 shows the dramatic change in viscosity with a modest change in temperature for glycerine and water solutions, as well as the relatively small change in density for changes in temperature.

As you can see in Figure B.2, the prepared working fluid samples were validated to have correct

viscosities compared to published and accepted data for water and glycerine solutions. The measured viscosity value was used for data analysis, because the impedance pump tests were performed at the same temperature (23°C) as the viscosity calibration measurements.

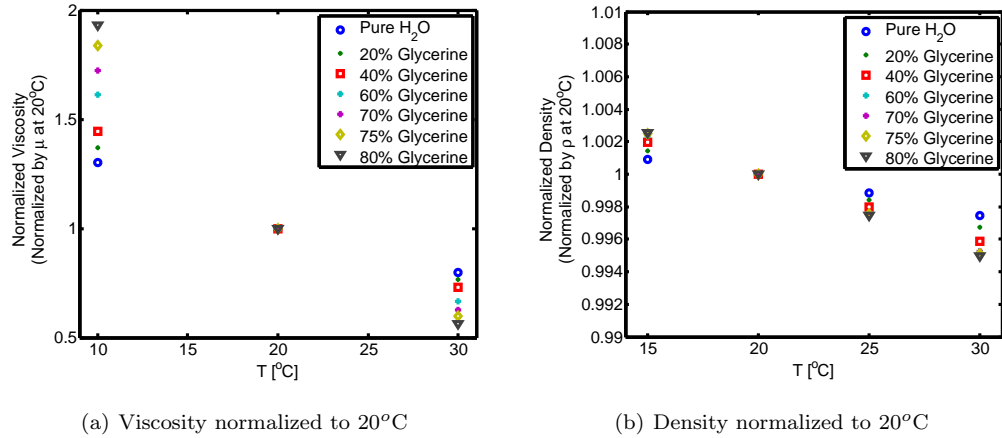


Figure B.1: Normalized viscosity and density showing the temperature dependence of water and glycerine solutions

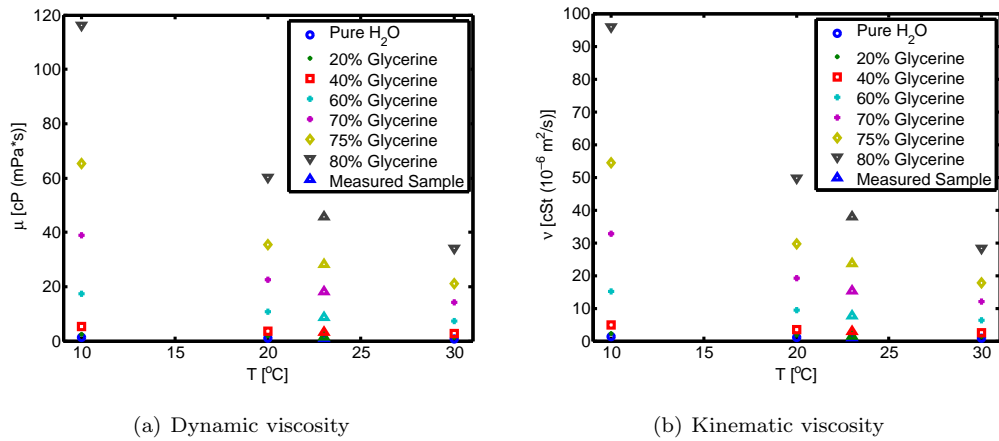


Figure B.2: Verification of measured sample viscosities compared to published data

## Appendix C

# DDPIV

The purpose of this appendix is to serve as a quick note describing the developments made to the calibration equations for out-of-plane measurement sensitivity in microscope-based or multiple lens DDPIV systems.

Willert and Gharib (1992) first proposed using a multiple aperture, single camera system for flow visualization, providing three-dimensional quantitative information. The out-of-plane sensitivity equations, Equation C.1 and C.2 for a single lens DDPIV system were originally calculated by Willert and Gharib (1992) and follow from the diagram in Figure C.1.

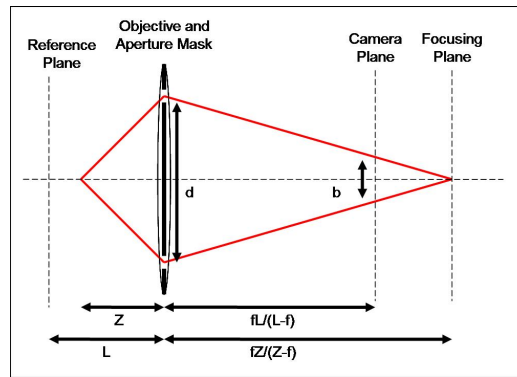


Figure C.1: Geometric diagram used for ray tracing and deriving the single lens out-of-plane DDPIV sensitivity equations in Willert and Gharib (1992)

$$b = MDL \left( \frac{1}{Z} - \frac{1}{L} \right) \quad (\text{C.1})$$

$$\frac{\partial b}{\partial z} = -\frac{MdL}{Z^2} \quad (\text{C.2})$$

In subsequent works applying the DDPIV technique to microscope-based optical systems (Yoon and Kim, 2006; Pereira et al., 2007; Lu et al., 2008), the individual roles of the objective lens and

tube lens were ignored and effective optical parameters were calculated from physical calibrations to satisfy Equation C.1 and C.2.

In some preliminary work investigating the ability of DDPIV to track the three-dimensional motions of a membrane in a planar valveless pump, a critical relationship was observed between the out-of-plane sensitivity and the total magnification of the microscope system. In all previous microscope-based DDPIV studies, the system's out-of-plane sensitivity was assumed to scale linearly with the system magnification  $M$  as shown in Equation C.2 (Yoon and Kim, 2006; Pereira et al., 2007; Lu et al., 2008). However, in the process of calibration, using different power microscope objectives, the sensitivity actually scaled as the square of the system magnification, shown in the calibration results in Figure C.2.

Objective	d	$\left. \frac{\partial b}{\partial Z} \right _{Z=L}$	$\left( \frac{\partial b}{\partial Z} \right)_{Z=L} - \left( \frac{\partial b}{\partial Z} \right)_{Z=L-1mm}$
4x	4 mm	0.014 pixels/ $\mu\text{m}$	1.6 %
	6 mm	0.021 pixels/ $\mu\text{m}$	1.6 %
	8 mm	0.028 pixels/ $\mu\text{m}$	1.6 %
10x	6 mm	0.134 pixels/ $\mu\text{m}$	1.7%
20x	4 mm	0.36 pixels/ $\mu\text{m}$	--

Figure C.2: Results of the out-of-plane sensitivity calibration for various objective lenses and aperture masks

This scaling behavior is a new and important result for all multiple-lens-based DDPIV systems. The new sensitivity equations, Equation C.3, C.4, and C.5, can be derived in a similar manner to that from Willert and Gharib (1992), using the diagram in Figure C.3. Equation C.5 shows that the out-of-plane measurement sensitivity should scale with the inverse of the square of the objective lens focal length. In microscopes, the magnification is changed by switching the objective lens and keeping the tube lens fixed. Thus, the result of scaling with the square of the system magnification is explained.

$$b = -df_t w \left( \frac{1}{f_o^2 + f_o w} \right) \quad (\text{C.3})$$

$$M = \frac{f_t}{f_o} \quad (\text{C.4})$$

$$w \ll f_o : b \approx -df_t w \left( \frac{1}{f_o^2} \right) \quad (\text{C.5})$$

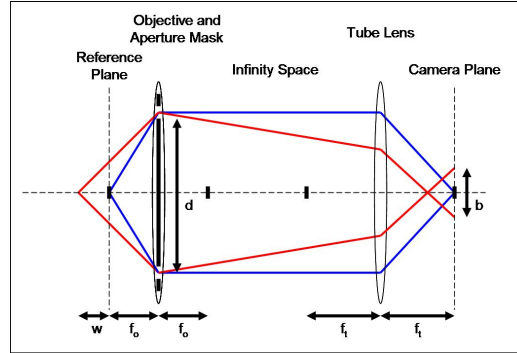


Figure C.3: Geometric diagram used for ray tracing and deriving the double lens (microscope) out-of-plane DDPIV sensitivity equations

## Bibliography

- J. Lu, F. Pereira, S. E. Fraser, and M. Gharib. Three-dimensional real-time imaging of cardiac cell motions in living embryos. *Journal of Biomedical Optics*, 13(1), 2008.
- F. Pereira, J. Lu, E. Castano-Graff, and M. Gharib. Microscale 3d flow mapping with mu dd piv. *Experiments in Fluids*, 42(4):589–599, 2007.
- C. E. Willert and M. Gharib. 3-dimensional particle imaging with a single camera. *Experiments in Fluids*, 12(6):353–358, 1992.
- S. Y. Yoon and K. C. Kim. 3d particle position and 3d velocity field measurement in a microvolume via the defocusing concept. *Measurement Science & Technology*, 17(11):2897–2905, 2006.

## Appendix D

# Wave Rectifying Water Channel: Liebau Phenomenon on a Free Surface

The following results were initially presented in the final report for Ae104-Spring 2007 (Meier and Kim, 2007).

### D.1 Experiment

Previous experimental and theoretical work on tubular impedance pumps gave us insight into the important experimental parameters in the Wave Rectifying Water Channel (WRWC). We wanted to easily vary excitation location, frequency, and offset as well as the boundary conditions at the wave reflection sites. For the WRWC we also suspected water depths above and below the suspended plate would be critical. The water depth above the suspended plate determined the velocity of the surface waves generated by the wave actuator. The water depth below the suspended plate affects the boundary conditions at the wave reflection sites as well as the overall system inertia.

For simplicity, we chose a pull type linear solenoid [12 V/9.8 W McMaster-Carr] for our wave actuation system. The frequency response of the solenoid was limited by the fact that the down stroke of the solenoid was driven by gravity. The maximum frequency we could achieve using a square wave input voltage with 50% duty cycle to run the solenoid was 2.8 Hz at a stroke length of 0.8 cm. It should be noted that the actual displacement of the solenoid did not have a duty cycle of 50% due to the voltage driven upstroke and gravity driven down stroke of the plunger. The resulting excitation was impulsive by nature.

Our excitation frequency range largely dictated the length scales of our water tunnel. We calculated an expected shallow water wave speed of  $c = 41.4$  cm/s for a water of depth of  $H = 1.75$

cm on top of the suspended plate, based on the shallow water wave speed equation,  $c = \sqrt{g * h}$ , where  $g = 9.8 \text{ m/s}^2$ . We chose the tank length to be 53.34 cm so that the free surface waves would travel the length of the tunnel in approximately one second and resonant frequencies for our setup would be on the order of 1 Hz. This time scale compliments our excitation frequency range of 0 to 2.8 Hz. We chose a tank width of 10.16 cm so that wall effects could be ignored and the flow could be assumed to be roughly two-dimensional, but at the same time not make the tank so large that filling and emptying would become cumbersome. Figure D.1 shows a dimensioned schematic of the water tunnel used for the frequency sweep study.

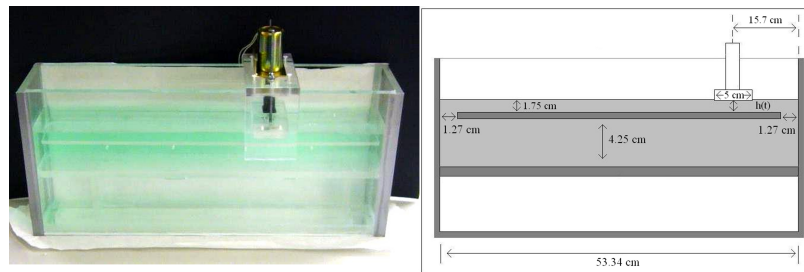


Figure D.1: Water tunnel dimensions.  $h(t)$  has a minimum value of 1 cm and a maximum value of 1.8 cm

## D.2 Wave Generation and Data Collection

The actuation solenoid was controlled with a function generator [HP 3314A] and high current amplifier [Crown DC300A]. The input waveform to the amplifier was a square wave with 320 mV amplitude, 320 mV offset, and 50 % duty cycle. Thus, the max voltage was 660 mV and the minimum voltage was 0 mV before the amplifier and 12.8 V and 0 V after the amplifier. Mechanical stops were employed to ensure a constant amplitude excitation across all frequencies. It is important to again note that the actual solenoid motion was not exactly 50 % duty cycle, because the down stroke of the piston was driven by gravity for all frequencies. For every test, the solenoid was started and the system was given at least 30 seconds to adjust to the periodic excitation in order to ensure that transient effects were not a factor.

Initially, we used simple dye visualization to determine the direction and relative velocity of the flow. We then employed DPIV to get quantitative information about the oscillatory nature of the flow. Our DPIV setup utilized 100  $\mu\text{m}$  fluorescent polystyrene particles, a green laser sheet from a low power laser ( $\approx 5\text{mW}$ ) and cylindrical lens, and a Uniq UG-1030 CCD camera. We performed DPIV of the flow beneath the suspended plate, measuring the full 2-D flow field from the bottom of the tank to the bottom of the submerged plate. Images were captured at 30 frames per second,

allowing us to get time resolved velocity field measurements at 15 Hz. We then multiplied that 2-D flux by the width of the channel to obtain an approximate flow rate. There is some small error introduced by not considering the boundary layer caused by the side walls of the tank, but for the remainder of the paper, this calculation is used to determine flow rate in all cases.

We also used a Redlake MDSC MotionMeter500 high speed camera to determine the actual wave speed and amplitude on the top of the suspended plate. The theoretical wave speed for the shallow water waves in our tank was 41.4 cm/s with a water depth of 1.75 cm. During the experiment, we determined the fully developed waves had an amplitude of approximately 0.3 cm and a velocity of 45 cm/s.

### D.3 Frequency Sweep Results

Several flow regimes exist beneath the suspended plate for varying excitation frequencies. Flows ranged from purely oscillatory with no net flow to oscillatory unidirectional flow. The nature of the flow was a strong function of the input excitation frequency, therefore we performed a parametric sweep of input frequencies from 1Hz to 2.8 Hz in 0.1 Hz increments. The flow rate vs. time at steady state was measured for each excitation frequency, and the system response (i.e. average flow rate and AC component) for each frequency was compared. The four frequency cases shown in Figure D.2 represent four distinct flow regimes. For 0.5 Hz and 1.5 Hz cases, the flow oscillates with positive and negative velocity, but with very different amplitudes and small mean velocity. For the 2.2 Hz case, the flow is counter-clockwise with a relatively high average velocity, and for the 2.8 Hz case, the flow is clockwise. The excitation amplitude was held constant for all four of these cases.

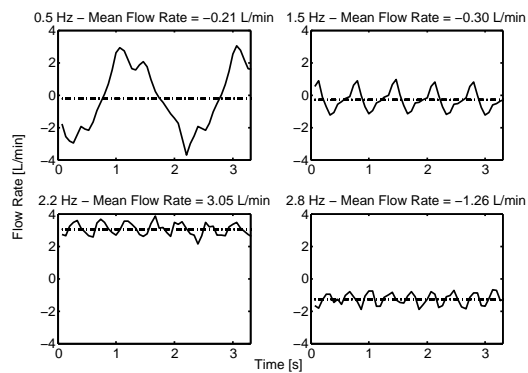


Figure D.2: A variety of flow regimes exist in the WRWC when only the input frequency is varied

As would be expected, the dominant frequency of the AC component of the flow beneath the plate matches the actuation frequency, however in some cases higher frequency flow behavior is

also evident. In Figure D.2, the flow corresponding to 0.5 Hz actuation clearly shows frequency components above 0.5 Hz. This frequency content could be a result of the impulsive nature of the actuation, or potentially a resonance due to one of the characteristic length scales in the system: channel length, channel width, channel depth, or excitation location for example.

After completing the frequency sweep, we were able to analyze the flow behavior and frequency response of the system. Figure D.3 shows the flow rate around the suspended plate as a function of the excitation frequency. An envelope representing the oscillatory component of the flow is also shown to help recognize different flow regimes.

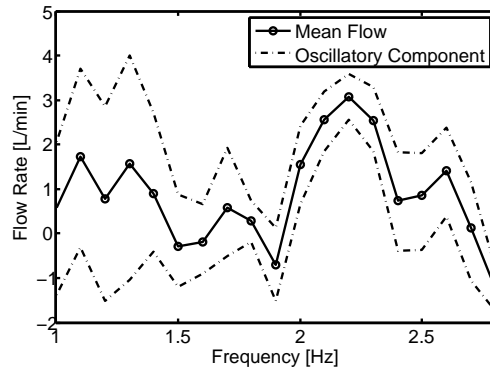


Figure D.3: Frequency response of the WRWC showing both the mean flow and the amplitude of the oscillatory component

Figure D.4 shows the result of normalized the flow rate around the plate by the rate of fluid displacement of the actuation plunger.

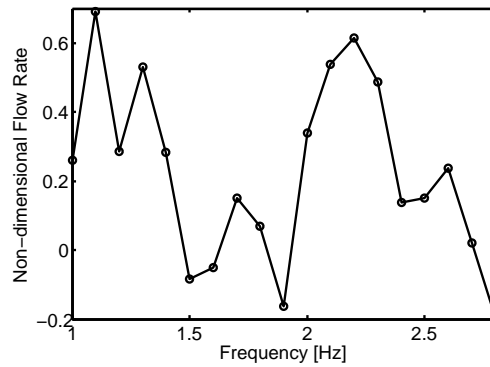


Figure D.4: The flow rate in the WRWC normalized by the rate of fluid displacement of the plunger

Figure D.5 shows the result of increasing the amplitude of the displacement of the actuation plunger. The WRWC shows many of the same behaviors as valveless pumps created using elastic

membranes. The WRWC serves as a proof of concept for valveless pumping in a system with a free surface.

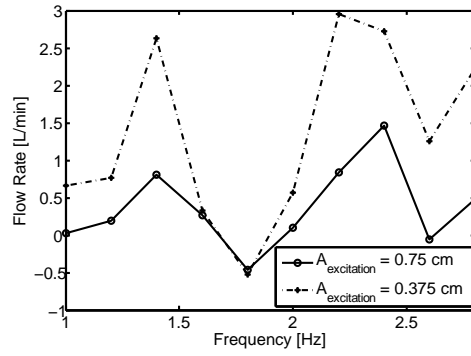


Figure D.5: Changing the amplitude of the plunger motion has similar effects to tube based impedance pumps

## Bibliography

J. Meier and D. Kim. An impedance driven water tunnel. Ae104 Final Report, May 2007.

## Appendix E

# Pump Behavior with Valves

To test the effects of placing valves inline with a valveless pump, two Qosina-80057 duckbill check valves were used in four different orientations inline with a 2 cm long thick-walled Allied Biomedical tube. The valve was first characterized using a large syringe to provide suction and driving pressure to determine the cracking pressure and flow resistance of the valve. Figure E.1 shows the result of this characterization: a cracking pressure for the valve of approximately 0.45 kPa and a flow resistance of approximately 0.05 kPa/(mL/min).

### E.1 Valve Characterization

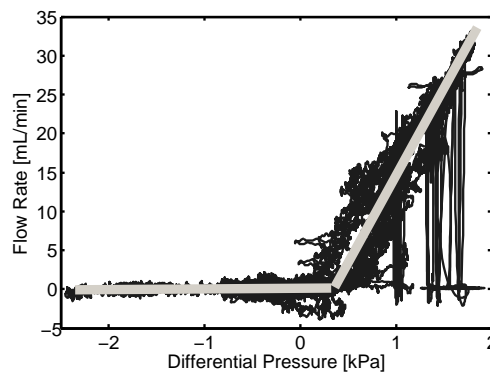


Figure E.1: Characterization of the Qosina-80057 Duckbill Check Valve.

### E.2 Effect of Single and Multiple Valves on Performance

In an attempt to preserve a symmetric flow loop, extra lengths of tubing were added to either side of the valveless pump that could be replaced by one of the Qosina duckbill valves. Figure E.2 shows

the performance of the thick-walled valveless pump with these extra lengths of tubing, but no valves in place.

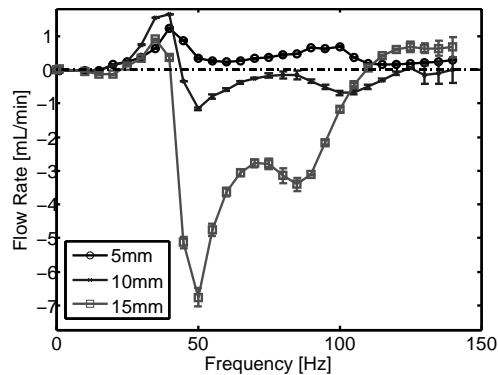


Figure E.2: Thick-walled AB 2 cm long tube excited at various locations with dummy tubing in place where valves can be added

The valves were then placed in various orientations with respect to the pump and the pump performance was retested. Figure E.3 shows a summary of these preliminary tests. When the valve was placed on the left side, the direction of the valve meant that it was upstream of the pump. Conversely, when the valve was placed on the right side, the direction of the valve meant that it was downstream of the pump. Some quick observations can be made from Figure E.3.

- The valves rectify all flow into the direction allowed by the valves, with one exception in the case of the valve upstream of the pump excited at a location of  $x = 15$  mm. This backward flow across the valve was verified by observation of the motion of microbubbles in the flow loop. It is believed that the complex dynamics and phase difference of the oscillatory pressure and flow signal allowed for this valve leakage to take place.
- Placing a valve downstream of the pump increases the maximum net flow rate generated when compared to the original system.
- Having valves both upstream and downstream of the pump is less beneficial than having only one valve downstream of the pump. This is likely due to the increased flow resistance across each valve.

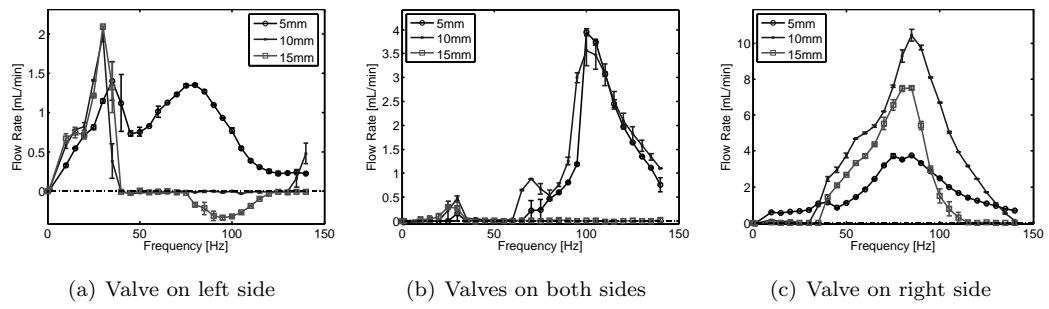


Figure E.3: Thick-walled AB 2 cm long tube excited at various locations with various valve configurations